Effect of Horizontal Resolution on the Simulation of Tropical Cyclones in the Chinese Academy of Sciences FGOALS-f3 Climate System Model

Jinxiao Li[1], Qing Bao[1], Yimin Liu[1], Lei Wang[1,5], Jing Yang[2,3], Guoxiong Wu[1], Xiaofei Wu[4], Bian He[1], Xiaocong Wang[1], Xiaoqi Zhang[6,1], Yaoxian Yang[1], Zili Shen[7,1]

[1] State Key Laboratory of Numerical Modeling for Atmospheric Sciences and Geophysical Fluid Dynamics, Institute of Atmospheric Physics, Chinese Academy of Sciences, Beijing 100029, China
[2] State Key Laboratory of Earth Surface Processes and Resource Ecology, Faculty of Geographical Science, Beijing Normal University, Beijing 100875, China
[3] Southern Marine Science and Engineering Guangdong Laboratory, Guangzhou 511458, China
[4] School of Atmospheric Sciences/Plateau Atmosphere and Environment Key Laboratory of Sichuan Province, Chengdu University of Information Technology, Chengdu 610225, China
[5] University of Chinese Academy of Sciences, Beijing 100049, China
[6] School of Atmospheric Sciences, Nanjing University of Information Science and Technology, Nanjing 210044, China
[7] Collaborative Innovation Center on Forecast and Evaluation of Meteorological Disasters, Nanjing University of Information Science and Technology, Nanjing 210044, China

Correspondence to: Qing Bao (baoqing@mail.iap.ac.cn)

Abstract. The effects of horizontal resolution on the simulation of tropical cyclones were studied using the Chinese Academy of Sciences FGOALS-f3 climate system model from the High-Resolution Model Intercomparison Project (HighResMIP) for the Coupled Model Intercomparison Project Phase 6 (CMIP6). Both the low-resolution (about 100 km resolution) FGOALS-f3 model (FGOALS-f3-L) and the high-resolution (about 25 km resolution) FGOALS-f3 (FGOALS-f3-H) model were used to achieve the standard Tier 1 experiment required by the HighResMIP. FGOALS-f3-L and FGOALS-f3-H have the same model parameterizations with the exactly the same parameters. The only differences between the two models are the horizontal resolution and the time step. The performance of FGOALS-f3-H and FGOALS-f3-L in simulating tropical cyclones was evaluated using observations. FGOALS-f3-H (25 km resolution) simulated more realistic distributions of the formation, movement and intensity of the climatology of tropical cyclones than FGOALS-f3-L at 100 km resolution. Although the number of tropical cyclones increased by about 50% at the higher resolution and better matched the observed values in the peak month, both FGOALS-f3-L and FGOALS-f3-H appear to replicate the timing of the seasonal cycle of tropical cyclones. The simulated average and interannual variabilities of the number of tropical cyclones and the accumulated cyclone energy were both significantly improved from FGOALS-f3-L to FGOALS-f3-H over most of the ocean basins. The characteristics of tropical cyclones (e.g., the average lifetime, the wind–pressure relationship and the horizontal structure) were more realistic in the simulation using the high-resolution model. The possible physical linkage between the performance of the tropical cyclone simulation and the horizontal resolution were revealed by further analyses. The improvement in the response between the El Niño–Southern Oscillation and the number of tropical cyclones and the accumulated cyclone energy in FGOALS-f3

contributed to the realistic simulation of tropical cyclones. The genesis potential index and the vorticity, relative humidity, maximum potential intensity and the wind shear terms were used to diagnose the effects of resolution. We discuss the current insufficiencies and future directions of improvement for the simulation of tropical cyclones and the potential applications of the FGOALS-f3-H model in the sub-seasonal to seasonal prediction of tropical cyclones.

1 Introduction

Tropical cyclones are extreme weather phenomena characterized by intense wind speeds and heavy rainfall. Although tropical cyclones alleviate coastal droughts, they can also cause severe economic losses and significant human casualties (Mendelsohn et al., 2012; Aon, 2018). Against the current background of global climate change, the effective simulation, prediction and projection of global tropical cyclone activity is challenging, but essential for disaster prevention and mitigation (Emanuel, 2017).

The simulation of tropical cyclones in global climate models (GCMs) is challenging in terms of both resolution and physical processes. Tropical cyclone-like structures appeared in early GCMs and Manabe et al. (1970), Bengtsson et al. (1982), Krishnamurti et al. (1989), Broccoli and Manabe (1990), Wu and Lau (1992) and Haarsma et al. (1993) were pioneers in using objective feature-tracking approaches to study simulated tropical cyclones. However, the low-resolution, incomplete parameterization of the physical processes in these early GCMs meant that their performance in simulating tropical cyclones was limited. For this reason, statistical methods were used to study the climatology of tropical cyclones. Camargo et al. (2013) found that the simulation of the frequency of tropical cyclones in the Coupled Model Intercomparison Project 5 (CMIP5) was much lower than in the observations. This was mainly due to the cold biases in the sea surface temperature, which amplified the uncertainty in future projections. Emanuel (2013) designed a downscaling method to reduce the uncertainty in projections of tropical cyclone activity.

The horizontal and vertical resolutions of climate system models have increased over the last few decades in line with the complex parameterization of the physical processes. As a result, more refined details (e.g., tropical cyclones and tropical waves) can now be resolved. Regional climate system models with smaller spatial scales and lower computing costs can now be used to simulate tropical cyclones. Knutson et al. (2007) used a high-resolution regional model to simulate tropical cyclone activity in the northern Atlantic Ocean. The structure and interannual variability of the simulated tropical cyclones have a high fidelity with the observations. There has also been a significant increase in the resolution of GCMs (Kim et al., 2014; Small et al., 2014; Li and Sriver, 2018; Scoccimarro et al., 2017; Balaguru et al., 2020). Oouchi et al. (2016) used a 20 km mesh global atmospheric model to simulate tropical cyclone activity in a warming climate and found that the high-resolution GCM could not only describe the details of typhoons very well, but also captured the variability of tropical cyclones. Zhao et al. (2009), Knutson et al. (2010), Murakami et al. (2012), Manganello et al. (2012), Strachan et al. (2013) and Zarzycki et al. (2015) showed that high-resolution GCMs can simulate many of the characteristics of tropical cyclones. The uncertainty in simulating

tropical cyclones has been reduced with an increase in resolution, the reasonable parameterization of the physical processes and improvements in the downscaling method (Walsh et al., 2015, 2016; Camargo et al., 2016).

The increase in the horizontal resolution of GCMs has led to significant changes in the simulation of the variability of tropical cyclones. The changes can be broadly attributed to two reasons: (1) changes in the large-scale factors; and (2) the development of physical process parameterization and air–sea coupling related to the simulation of tropical cyclones. High-resolution GCMs need to not only give a better description of the structure of tropical cyclones, but should also simulate well the relationship between tropical cyclones and large-scale variabilities—for example, the El Niño–Southern Oscillation (ENSO), the Madden–Julian oscillation, wind shear and vorticity, and humidity—which is crucial in reducing the uncertainties in the simulation and prediction of tropical cyclones (Manganello et al., 2012, 2016; Zhang et al., 2016; Delworth et al., 2020). Previous studies have shown that there are significant changes in the ENSO as the horizontal resolution of GCMs increases (Philander et al., 1992; Kuntson et al., 1997; Schneider et al., 2003; Masson et al., 2012; Larson et al., 2013; Meehl et al., 2020) and the simulation results are mostly positive. However, these improvements in predicting the ENSO with an increase in horizontal resolution did not lead to improvements in the relationship between the ENSO and tropical cyclones (Matsuura et al., 1999; Bell et al., 2014; Krishnamurthy et al., 2016). There is also a relationship between the Madden–Julian oscillation and tropical cyclones (Liebmann et al., 1994; Hall et al., 2001; Camargo et al., 2008, 2009; Zhang et al., 2013; Klotzbach et al., 2014).

As the horizontal resolution in the models increases, some key parameters in the physical parameterizations are tuned to give a better performance (Bacmeister et al., 2013; Roberts et al., 2020)—for example, Lim et al. (2015) found that an increase in the threshold of minimum entrainment led to increasing tropical cyclone activity and Murakami et al. (2012) found that the constrained convective heating in the convective scheme induced intense grid-scale upward motion and promoted large-scale condensation, which favored the development of a more intense tropical cyclone. These artificial tuning methods might introduce more uncertainties in terms of the effects of resolution, giving rise to conclusions that are ambiguous to the tropical cyclone research community. In addition, considering the air–sea coupling process will also affect the simulation performance of tropical cyclone activities, especially with respect to the intensity. Scoccimarro et al. (2017) found that an increased horizontal resolution of the model components was not sufficient to simulate intense and fast-moving tropical cyclone events and that air–sea coupling with a higher coupling frequency helps to improve the performance of simulations of tropical cyclone intensity.

The impacts of horizontal resolution on the simulation of tropical cyclones were studied using the Chinese Academy of Sciences Flexible Global Ocean–Atmosphere–Land System Finite-Volume Version 3 (FGOALS-f3) model, which was developed by the State Key Laboratory of Numerical Modeling for Atmospheric Sciences and Geophysical Fluid Dynamics (LASG), Institute of Atmospheric Physics (IAP). The simulated tropical cyclones in FGOALS-f3 were introduced first, then the outputs of FGOALS-f3-L and FGOALS-f3-H were used to reveal the influence of horizontal resolution on these simulations. The latest version of FGOALS-f3 participated in the CMIP6 (Eyring et al. 2016), DECK and MIPs endorsements (Zhou et al. 2016; He et al. 2019, 2020; Haarsma et al. 2016). FAMIL2 is the atmospheric component of the FGOALS-f3

climate system model. Li et al. (2019) evaluated the simulation performance of tropical cyclone activity in the latest generation atmospheric general circulation models from the LASG–IAP (FAMIL2) using a coarse resolution with standard AMIP experiments. Although FAMIL2 is able to reproduce many aspects of the activities of tropical cyclones with a horizontal resolution of 1°, there is still some room for improvement in simulating tropical cyclones, such as the weak intensity of tropical cyclones, fewer tropical cyclones in the peak month in the northern Atlantic and eastern Pacific oceans, and inaccurate large-scale factors. Therefore, the HighResMIP configuration has been applied to both the low- and high-resolution FGOALS-f3. Both model versions retained the exact model physics and parameters and the only differences were the horizontal resolution and model time step, which better meet the rule of HighResMIP: "The experimental set-up and design of the standard-resolution experiments will be exactly the same as for the high-resolution runs." This study aimed to address the following issues: (1) the impacts of horizontal resolution on the simulation of global tropical cyclones in a climate system model; and (2) the possible physical linkages between the horizontal resolution and the simulated tropical cyclones.

This paper is organized as follows. Section 2 introduces the model, data and methods used in this study. Section 3 shows the performance of simulated tropical cyclones in both FGOALS-f3-L and FGOALS-f3-H. Section 4 introduces the possible reasons for the improvement in the simulation of tropical cyclones with an increased horizontal resolution. Section 5 discusses the impact of physical parameterization and air–sea coupling on the simulated tropical cyclones in GCMs, then discusses the potential value-added effect of large-scale factors related to simulated tropical cyclones when the horizontal resolution is increased from the HighResMIP models. Section 6 summarizes our results.

2 Model, data and methods

2.1 Description of FGOALS-f3

FGOALS-f3 is the latest version of the Chinese Academy of Sciences climate system model and was designed for CMIP6. The FGOALS-f3 model consists of four components: (1) an atmospheric component; (2) an oceanic component; (3) a land surface component; and (4) a sea ice component. The atmospheric component is the Finite-volume Atmospheric Model Version 2.2 (FAMIL2.2) (Zhou et al., 2015; Bao et al., 2018, 2020; Li et al., 2019; He et al., 2019), which is the successor to the atmospheric general circulation model of the Spectral Atmosphere Model of LASG (SAMIL) (Wu et al., 1996; Bao et al., 2010, 2013). The oceanic component is the LASG/IAP Climate System Ocean Model Version 3 (LICOM3) (Liu et al., 2012). Orthogonal curvilinear coordinates and a tripolar grid are used in LICOM3 and the horizontal resolution can vary flexibly between 1° and 1/20°. A new advection scheme has also been updated in LICOM3 (Yu et al., 2018). The land surface component is the Community Land Model Version 4.0 (CLM4) (Oleson et al., 2010; Lawrence et al. 2011) with the processes from the dynamic global vegetation model in CLM4.0 used in FGOALS-f3-L/H turned off. The sea ice component is the Los Alamos Sea Ice Model Version 4.0 (CICE 4.0; Hunke et al. 2008; Hunke & Lipscomb, 2010). These four components are coupled by the Version 7 coupler in the CESM (Craig et al., 2012). Li et al. (2019) introduced the atmospheric component FAMIL2 in detail and carried out some tuning to achieve stability in long-term coupled integrations (defined as FAMIL2.2).

Table 1 shows that the finite-volume cubed-sphere dynamical core (FV3) (Lin, 2004; Putman and Lin, 2007; Voosen, 2017) is used as the dynamical core in FAMIL2.2. The University of Washington moist turbulence parameterization (Park & Bretherton, 2009) is also used in FGOALS-f3. This is a non-local, high-order closure scheme and uses the diagnosed turbulent kinetic energy to determine the eddy diffusivity in turbulence. The Resolving Convective Precipitation (RCP) parameterization (Bao and Li, 2020) is used, which involves calculating the microphysical processes in the cumulus scheme for both deep and shallow convection; six species are considered, similar to the Geophysical Fluid Dynamics Laboratory (GFDL) cloud microphysics scheme (Zhou et al., 2019). The gravity wave drag scheme (Palmer et al., 1986), the cloud fraction diagnosis scheme (Xu & Randall, 1996) and the radiative transmission scheme (Clough et al., 2005) are also considered.

The vertical layers of FGOALS-f3-L and FGOALS-f3-H are both set to 32, whereas the horizontal resolutions of FGOALS-f3-L and FGOALS-f3-H are C96 (about 100 km) and C384 (about 25 km), respectively (Table 2). To maintain the stability of the integration for the dynamical core, the two parameters k_split and n_split included in FV3 are different in FGOALS-f3-L and FGOALS-f3-H. k_split is the number of vertical remapping operations per physical time step in the dynamical integration and n_split is the number of small dynamic (acoustic) time steps between the vertical remapping operations, which will affect the stability of the integration when the horizontal resolution of the model is changed. Considering that FGOALS-f3-H requires more frequent vertical remapping, k_split and n_split are set to 6 and 15, respectively (they are 2 and 6, respectively, in FGOALS-f3-L). The time steps of the physical processes are both set to 30 minutes, but the update frequency of radiative transmission and the minimum time step of the microphysics scheme in both FGOALS-f3-L and FGOALS-f3-H are 1 h and 150 s, respectively. Li et al. (2017) tested the computing performance between FGOALS-f3-L and FGOALS-f3-H using the Supercomputer Tianhe-2 and the results indicated a high computing speed-up and low computing costs when the number of parallel processes was increased.

2.2 Datasets

FGOALS-f3 participated in CMIP6 DECK (Eyring et al., 2016), the Global Monsoons Model Intercomparison Project (GMMIP; Zhou et al. 2016; He et al. 2019) and the High-Resolution Model Intercomparison Project (HighResMIP; Haarsma et al. 2016). The datasets from CMOR for the CMIP6 HighResMIP are in a standard format. The experimental design satisfies the requirement for HighResMIP Tier 1. Two resolutions of FGOALS-f3 are used to compare the simulation of tropical cyclone activities at different resolutions. To identify the impact of resolution, there was no tuning of the parameterization of the physical processes between FGOALS-f3-L and FGOALS-f3-H. The time period 1991–2014 is extracted to avoid the uncertainties in the pre-satellite era in the observations.

The International Best Track Archive for Climate Stewardship v03r10 (IBTrACS; Knapp et al., 2010) is used as the observational dataset. IBTrACS is a multisource dataset and includes the RSMC Tokyo, Chinese Meteorological Administration–Shanghai Typhoon Institute (Ying et al. 2014) and the National Hurricane Center data sources. To provide a fair comparison, transformation from the 10-min-averaged maximum sustained wind to the 1-min-averaged maximum sustained wind is needed and the relevant coefficient is set to 0.88 (Manganello et al., 2012; Knapp et al. 2010; Li et al. 2019).

The European Centre for Medium-Range Weather Forecasts ERA-Interim reanalysis dataset (Dee et al., 2011) (resolution 0.75°), the National Centers for Environmental Prediction Global Forecast System (GFS) reanalysis dataset (resolution 0.25°) and the Global Precipitation Measurement (GPM) dataset (resolution 0.25°) (Hou et al., 2014) for the time period 1991–2014 are used as the observations to quantitatively evaluate the tropical cyclones simulated in FGOALS-f3.

2.2 Tracking algorithms

An objective feature-tracking approach is used to detect the model-generated tropical cyclones based on the 6-h outputs of FGOALS-f3-L and FGOALS-f3-H. According to the tracking scheme (Table 3), the sea-level pressure, warm core (the temperature anomaly averaged between 300 and 500 hPa), 10 m wind and the 850 hPa absolute vorticity are used to diagnose the tropical cyclone activity, which is similar to the method used in the climate system model of the GFDL (Zhao et al. 2009; Chen & Lin 2013; Xiang et al. 2015). Li et al. (2019) used this scheme to evaluate the simulated performance of tropical cyclones in FAMIL2 and showed a consistent performance. The wind speed thresholds between FGOALS-f3-L and FGOALS-f3-H are consistent with the relationship between the horizontal resolution of the models and the tropical cyclone detection algorithms (Walsh et al., 2007).

3 Results

3.1 Global climatology of tropical cyclone track density

The climatology of simulated tropical cyclones is the first step in testing the performance of the model. Zhao et al. (2009) used a GFDL GCM with a 50 km horizontal resolution to simulate global tropical cyclone activity and obtained a negative bias in the number of tropical cyclones in the eastern Pacific, northern Atlantic and southern Indian oceans. These biases also appeared in the low-resolution models participating in the US CLIVAR Working Group on Hurricanes (Walsh et al., 2015). Figure 1a and 1b show the tracks and intensities of global tropical cyclones in the FGOALS-f3-L and FGOALS-f3-H simulations, respectively. The definition of the intensity follows the Saffir–Simpson intensity scale (Simpson & Saffir, 1974). The negative biases of the tracks of tropical cyclones in FGOALS-f3-L (Figure 1a) improves when the horizontal resolution increases from 100 to 25 km (Figure 1b) relative to IBTrACS. Table 4 shows the observed and simulated average number of tropical cyclones, both globally and by ocean basin. The results in Table 4 indicate that the value-added effect of tropical cyclone counts from the increased horizontal resolution is seen globally.

The improvement is also clearly shown in Figure 2 and the differences in track densities between FGOALS-f3-H and FGOALS-f3-L reflect a positive distribution in the global basin (Figure 2c). The biases in the track densities between the simulation and IBTrACS are improved when the horizontal resolution is increased from 100 km (Figure 2a) to 25 km (Figure 2b), especially in the low-latitude basins where tropical cyclones form. Negative biases between FGOALS-f3-L and IBTrACS appear in the mid-latitudes of the western Pacific and northern Atlantic oceans, but positive biases between the FGOALS-f3-

H and IBTrACS also appear in these areas, which means that there are more tropical cyclone events at higher latitudes in FGOALS-f3-H than in IBTrACS and the simulation in FGOALS-f3-L. This phenomenon also exists in the high-resolution GCMs that participated in the European Union Horizon 2020 project PRIMAVERA (Roberts et al., 2020). The biases in the large-scale factors (e.g., strong steering flow) related to the tropical cyclones in GCMs may lead to the simulated biases of tropical cyclone activities in the western Pacific and northern Atlantic oceans.

The negative biases in the intensities of tropical cyclones are also improved when the horizontal resolution is increased from 100 km (Figure 1a) to 25 km (Figure 1b), especially in the western Pacific and northern Atlantic oceans. The difference in wind speed densities between FGOALS-f3-L and FGOALS-f3-H (Figure 3c) shows a significant increase in the wind speed densities in the northern Atlantic, eastern Pacific and northern Indian oceans and the mid-latitude region of the western Pacific Ocean when the horizontal resolution is increased from 100 to 25 km. Similar to the pattern of track density anomalies (Figure 2), the biases in the wind speed densities between FGOALS-f3 and IBTrACS are improved when the horizontal resolution is increased from 100 to 25 km, but the positive biases are intensified in the mid-latitudes of the western Pacific and northern Atlantic oceans.

Figure 4 shows the pressure–wind pairs for each six-hourly measurement of tropical cyclones between FGOALS-f3 and IBTrACS. The results indicate that the simulated intensity of tropical cyclones is increased globally. These results also indicate that the spread of pressure–wind pairs in FGOALS-f3-L is narrow and there is a severe underestimation of intense tropical cyclone events at lower surface pressures and higher wind speeds in the western Pacific and northern Atlantic oceans, although this bias has been dramatically improved (Figure 4b, 4d).

The increased intensity of tropical cyclones in FGOALS-f3-H favors the apparent negative bias of the lifetime of tropical cyclones in FGOALS-f3-L when the horizontal resolution is increased. Figure 5 shows the average lifetime of tropical cyclones from 1991 to 2014. The average lifetime of tropical cyclones in the observations is about 8.5, 7.5, 7.5, 4, 6.1 and 7.5 days in the western Pacific, northern Atlantic, eastern Pacific, northern Indian, southern Indian, and southern Pacific oceans, respectively, and the simulation of the average lifetime of tropical cyclones is increased in these six basins when the horizontal resolution is increased from 100 to 25 km. For example, the simulated average lifetime of tropical cyclones increases from 6 to 7.4 days when the horizontal resolution is increased in the western Pacific Ocean.

删除了: 6.1

删除了: southern Indian

删除了: five

3.2 Seasonal cycles, interannual variability and accumulated cyclone energy of tropical cyclones

Evaluating the seasonal cycle and interannual variability of tropical cyclones in GCMs is an efficient way to verify the coordination between tropical cyclone activity and large-scale circulation patterns (Manganello et al., 2012; Camargo et al., 2016; Kuntson et al., 2019; 2020). Robert et al. (2020) found no uniform improvement in the seasonal cycle and interannual variability of tropical cyclones at increased horizontal resolutions, which means that there is a difference in coordination between tropical cyclone activity and large-scale circulation patterns in high-resolution GCMs. Figure 6 shows the seasonal cycle of tropical cyclones between IBTrACS, FGOALS-f3-L and FGOALS-f3-H and shows that FGOALS-f3-L gives a consistent underestimation of the seasonal cycle of tropical cyclones in the northern Atlantic, eastern Pacific, northern Indian,

southern Indian, and southern Pacific oceans. Neither the single peak in the number of tropical cyclones in the northern Atlantic (peak month September), eastern Pacific (peak month August) and southern Pacific (peak month February) oceans nor the double peak in the northern Indian Ocean (peak months May and November) could be reproduced in FGOALS-f3-L. There are two increases in the simulated number of tropical cyclones in the peak months of the northern Atlantic and eastern Pacific oceans and the characteristics of the seasonal cycle of simulated tropical cyclones are improved in the northern Indian, western Pacific and southern Pacific oceans as the horizontal resolution is increased from 100 to 25 km. Although FGOALS-f3-H can produce more tropical cyclone counts in the peak month in each basin, both FGOALS-f3-L and FGOALS-f3-H appeared to replicate the timing of the seasonal cycle when we normalized the results of the tropical cyclone seasonal cycle (Figure S1). Figure 7 shows the interannual correlation of the number of tropical cyclones between FGOALS-f3 and IBTrACS. The results show that the correlation coefficient is improved in each basin, which reflects the fact that the interannual variability between tropical cyclone activity and large-scale circulation patterns is harmonious.

Table 5 shows the observed and simulated averaged accumulated cyclone energy (ACE; Bell et al., 2000). ACE is a measure used by the National Oceanic and Atmospheric Administration in which the energy over the lifetime of a tropical cyclone is calculated for every six-h period:

$$\mathrm{ACE} = 10^{-4} \sum V_{\mathrm{m}}^2 \quad (1)$$

where V_{m} is the estimated sustained wind speed in knots.

Our results indicate that the negative biases of the ACE in FGOALS-f3-L are improved globally when the horizontal resolution is increased to 25 km. Figure 8 shows the interannual correlation of the ACE between FGOALS-f3 and IBTrACS. The results show that the correlation coefficient of the ACE between IBTrACS and the simulation is improved in each basin when the horizontal resolution is increased from 100 to 25 km. The increase in the number, lifetime and intensity of simulated tropical cyclones contributes to the increased correlation coefficient of the ACE (Camargo and Sobel, 2005).

3.3 Horizontal structure of tropical cyclones

Previous studies have shown that the horizontal resolution influences the horizontal structure of simulated tropical cyclones (Strachan et al., 2013; Murakami et al., 2012; 2013; Roberts et al., 2020). Manganello et al. (2012) compared the horizontal structure of the moisture content of tropical cyclones in GCMs between low (T511) and high (T2047) resolutions and found that the refined structure of the liquid component of tropical cyclones was simulated when the horizontal resolution was increased. Following the method of Manganello et al. (2012), the surface 10 m wind and daily precipitation rate for the 30 most intense tropical cyclones in FGOALS-f3-L (Figure 9a) and FGOALS-f3-H (Figure 9b) were combined. The results of the GFS (Figure 9c) and the GFS&GPM (Figure 9d) simulations are also shown for comparison. The results indicate that there is no prominent precipitation structure of tropical cyclones in FGOALS-f3-L, but there is a considerable improvement in the results with a horizontal resolution of 25 km. The eyewall and organized precipitation of tropical cyclones are apparent in the FGOALS-f3-H simulation. The main uncertainty is the position of extreme precipitation. The position of extreme precipitation appears 100 km east of the eyewall in the FGOALS-f3-H simulation (Figure 9b), but is 100 km south of the eyewall in the

删除了:

GFS&GPM datasets (Figure 9c). There is an apparent error in the angle compared with the radial distance for the simulated horizontal structure of tropical cyclones. Chen et al. (2006) found that the vertical wind shear and storm motion are the two most important factors contributing to rainfall asymmetries in tropical cyclones. The biases in the vertical wind shear and storm motion in FGOALS-f3 may affect the angle of the horizontal structure of tropical cyclones. The non-hydrostatic dynamical core used in FGOALS-f3 and the limited air–sea coupling processes (Emanuel et al., 2013; Kim et al., 2018) (AMIP) also contribute to the error.

4 Possible reasons for the simulated performance of tropical cyclones in FGOALS-f3

4.1 Modulation of tropical cyclone activity by the ENSO

There is a lot of evidence to suggest that the ENSO modulates the activity of tropical cyclones. Gray et al. (1984) found that tropical cyclone counts in the Atlantic Ocean are modulated by the ENSO. El Niño (La Niña) events enhanced (suppressed) westerly winds and led to stronger (weaker) vertical wind shear in the Atlantic basin, leading to an increase (decrease) in tropical cyclone counts. Camargo et al. (2004) found that the ACE in the western Pacific is positively correlated with ENSO indices. There are more intense and longer lived tropical cyclones in El Niño years than in La Niña years. Kim et al. (2011) found that the ENSO modulates tropical cyclone activity in the eastern Pacific Ocean. The track densities and genesis of tropical cyclones tend to be enhanced (suppressed) in eastern Pacific warming (cooling) years by strong (weak) westerly wind shear.

Figure 10 shows the average number of tropical cyclones and the ACE from El Niño, neutral and La Niña years. In the western Pacific basin (Figure 10a), there is no clear change in tropical cyclone counts compared with the variation of the ACE between El Niño and La Niña years. FGOALS-f3-H can capture these features in the observations; in particular, the simulation of the ACE is better than in FGOALS-f3-L. In the eastern Pacific basin (Figure 10b), FGOALS-f3 can capture the variation in tropical cyclone activities from El Niño to La Niña years, but the decreasing trend of tropical cyclone counts and the ACE in FGOALS-f3-L/H is weaker than in the observations. In the observations for the northern Atlantic basin (Figure 10c), there are more intense tropical cyclone events in La Niña years. FGOALS-f3 can reproduce the impact of the ENSO on tropical cyclone activity in the northern Atlantic Ocean and the simulated performance of tropical cyclones in FGOALS-f3-H is better than that in FGOALS-f3-L.

4.2 Large-scale environmental factors

The genesis potential index (GPI; Emanuel et al., 2004) is applied to detect the connection between the genesis of tropical cyclones and large-scale circulation patterns. Camargo et al. (2007) and Walsh et al. (2013) found that the correlation between the GPI and the variation of tropical cyclones in GCMs mainly depends on the horizontal resolution and the similarity between the GPI. The variation in tropical cyclones is increased when the horizontal resolution is increased. The GPI used in this work is defined as:

$$GPI = |10^5 vort850|^{3/2} \left(\frac{RH}{50}\right) \left(\frac{V_m}{70}\right) (1 + 0.1V_{shear})^{-2} \quad (2)$$

where *vort*850 is the 850 hPa absolute vorticity (s^{-1}), *RH* is the 600 hPa relative humidity (%), V_m is the maximum potential intensity (Emanuel, 1995) and V_{shear} is the magnitude of the wind shear between 850 and 200 hPa (m s^{-1}). V_m (the maximum potential intensity) is defined here as:

$$V_m = \frac{C_k T_s}{C_d T_0}(CAPE^* - CAPE^b) \quad (3)$$

where C_k is the exchange coefficient of the enthalpy, C_d is the drag coefficient, T_s is the sea surface temperature and T_0 is the mean outflow temperature. *CAPE** is the convective available potential energy of the air lifted from saturation at sea-level and $CAPE^b$ is the convective available potential energy of the boundary layer air.

Figure 11 shows the biases of the large-scale environmental factors related to tropical cyclone activity between FGOALS-f3 and the observations. The results indicate that the biases in the large-scale environmental factors are decreased in FGOALS-f3 when horizontal resolution is increased from 100 to 25 km, which is related to the biases in the simulated tropical cyclones. For example, the environmental vertical wind shear (VWS) is known to be one of the major factors in the generation and intensity of tropical cyclones (Gray, 1968; Wong and Chan, 2003). An excessive VWS in the eastern Pacific and northern Atlantic oceans can lead to the suppression of the generation and intensity of simulated tropical cyclones in these basins (Figure 11e), which is consistent with the results for the simulation of tropical cyclones in FGOALS-f3-L (Figure 3). The results in Figure 12 show the pattern correlation of each individual part of the GPI. P1 represents the equation $|10^5 vort850|^{3/2}$, P2 represents the equation $\frac{RH}{50}$, P3 represents the equation: $\frac{V_m}{70}$ and P4 represents the equation $(1 + 0.1V_{shear})^{-2}$. The results indicate that the pattern correlation coefficients are increased in the northern Indian (Figure 12a), western Pacific (Figure 12b), eastern Pacific ((Figure 12c) and northern Atlantic (Figure 12d) oceans, which is favored by the reduction in the bias of the large-scale circulation patterns.

5 Discussion

5.1 Impact of physical parameterization and air–sea coupling on tropical cyclones simulated in GCMs

An RCP scheme has been used in both the high- and low-resolution versions of FGOALS-f3 (Bao and Li, 2020; He et al., 2019; Li et al., 2019). The RCP scheme calculates convective and stratiform precipitation at the grid scale, which has the advantage of both scale-awareness and high computational efficiency. The parameterizations of physical processes in traditional GCMs are very sensitive to changes in resolution. In particular, convection and cloud processes are considered to be effectively resolved, which means that the assumptions and equations in low-resolution simulations are not suitable for high-resolution GCMs. As a result, the model convergence will be degraded as the resolution increases (Sakradzija et al., 2016). Simulated tropical cyclones are very sensitive to convection and cloud processes in GCMs (Zhao et al., 2012). The effective tuning of convection (Lim et al., 2015; Murakami et al., 2012), boundary condition (Zhang et al., 2017) and microphysics (Chutia et al., 2019) parameterizations contribute to improvements in the intensity, number, track and structure

of simulated tropical cyclone. Although a fixed parameterization scheme combined with a fine grid will clearly improve the simulation of tropical cyclone activity, the effect of resolution will be amplified. According to this study, GCMs with scale-aware parameterizations still slightly underestimate the intensity of tropical cyclones at 0.25° resolution (Figure 1). In addition, air–sea exchange and non-hydrostatic processes are both important in enhancing the intensity of tropical cyclones (Ma et al., 2017). Emanuel and Sobel (2013) found that the absence of air–sea coupling can lead to potentially large imbalances in the surface energy budget, which is not conducive to the development of tropical cyclones.

5.2 Large-scale environmental factors from HighResMIP models

Our results (Figure 11) show a clear improvement in the large-scale factors related to the generation and development of tropical cyclones when the horizontal resolution is increased from 100 to 25 km in FGOALS-f3. It is worth exploring whether these improved large-scale factors are common to all the GCMs participating in HighResMIP. The eight models participating in the HighResMIP Tier1 were selected (Table 6) to calculate the GPI. The results indicate that the GPI patterns in high-resolution models (Figure 13b) are closer to the observations (Figure 13a) than those in the standard-resolution models (Figure 13c), which means that the large-scale factors related to tropical cyclones are improved when the horizontal resolution of the models is increased. However, the difference between the tracking algorithms—such as TRACK (Hodges et al., 2017), TSTORM (Zhao et al., 2009) and TempestExtremes (Ullrich et al., 2017, 2021)—are also an important factor in the uncertainties in tropical cyclone simulations. Cross-validation of the performance of tropical cyclone simulations with multiple tracking algorithms is necessary in future research (Roberts et al., 2020).

6 Summary and conclusions

The impacts of horizontal resolution on the simulation of tropical cyclones were studied with the latest version of FGOALS-f3, which participated in the CMIP6 HighResMIP (Haarsma et al., 2016). Li et al. (2019) evaluated the simulation performance of tropical cyclone activity in FAMIL2 (resolution about 100 km), which is the atmospheric component of FGOALS-f3 (He et al., 2019) and put forward the idea that the simulated performance of tropical cyclones is improved with the increased horizontal resolution in FAMIL2. We examined these hypotheses and our main findings and conclusions are as follows.

1. There are improvements in the track and intensity of global tropical cyclones in the FGOALS-f3 simulations when the horizontal resolution is increased from 100 (FGOALS-f3-L) to 25 km (FGOALS-f3-H) and the negative biases in tropical cyclone genesis are improved in the eastern Pacific and northern Atlantic oceans. Quantitative comparisons between the track density of tropical cyclones between FGOALS-f3-L, FGOALS-f3-H and IBTrACS show that the negative biases in the tropical cyclone track densities at low latitudes are alleviated. The surface wind speed of tropical cyclones is increased when the horizontal resolution is increased and this change in FGOALS-f3-H is closer to the observations. The improvement in the intensity of tropical cyclones in FGOALS-f3-H is easier to detect in the pressure–wind pairs of

tropical cyclones. A wide spread of pressure–wind pairs is simulated in FGOALS-f3-H and the biases in the pressure–wind pairs are improved relative to the observations.

2. The global lifetimes of tropical cyclones in FGOALS-f3-H are increased compared with the FGOALS-f3-L simulation, especially in the western Pacific, northern Atlantic, eastern Pacific and southern Pacific oceans. The increase in the intensity of tropical cyclones in FGOALS-f3-H contributes to the improvement in the lifetime of tropical cyclones. In the seasonal cycle of tropical cyclones, only 50% of tropical cyclones are simulated in the peak month, but this bias is improved in FGOALS-f3-H compared with the observations. Both FGOALS-f3-L and FGOALS-f3-H appear to replicate the timing of the seasonal cycle. The average ACE and number of tropical cyclones in FGOALS-f3-H are close to the observations. The correlation of the annual number of tropical cyclones and the annual ACE of tropical cyclones are both improved in the western Pacific, northern Atlantic, eastern Pacific, southern Pacific and northern Indian oceans when the horizontal resolution is increased.

3. There is a significant improvement in the horizontal structure of tropical cyclones in FGOALS-f3 when the horizontal resolution is increased. The eyewall and the organized precipitation of tropical cyclones are apparent in the FGOALS-f3-H simulation and the main uncertainty is the position of extreme precipitation.

4. The possible reasons for the improvement in the simulated tropical cyclones are explained by the ENSO and large-scale environmental factors. FGOALS-f3 can reproduce the response between the ENSO and tropical cyclone activities, and the biases in the number of tropical cyclones and the ACE in FGOALS-f3-H are decreased. The large-scale factors and GPI biases between FGOALS-f3-L and FGOALS-f3-H are consistent with the biases in the simulated tropical cyclones, which means that the improvement in the large-scale environmental factors in FGOALS-f3 contributes to the simulation of tropical cyclones. This study shows that it is worth establishing a high-resolution coupled dynamic prediction system based on FGOALS-f3-H to improve the prediction skill of tropical cyclones on sub-seasonal to seasonal scales (Camp et al., 2018; Murakami et al., 2016). This dataset will be uploaded to the sub-seasonal to seasonal prediction project (Vitart, et al., 2018; Vitart et al., 2017).

Code and data availability

The model output of the FGOALS-f3 models for CMIP6 simulations used in this work has been uploaded to the Earth System Grid Fedration (ESGF) and users can access to these outputs freely. The DOI for CMIP6.HighResMIP.CAS.FGOALS-f3-H. highresSST-present is doi:10.22033/ESGF/CMIP6.3312 and the DOI for CMIP6.HighResMIP.CAS.FGOALS-f3-L. highresSST-present is doi:10.22033/ESGF/CMIP6.12009. The other output of GCMs participating in the HighResMIP (Table 6) are also distributed through the ESGF and the users can search it on the website at https://esgf-node.llnl.gov/projects/cmip6/ after simple registration. The source code of the model can be found at http://doi.org/10.5281/zenodo.4588109. All the source code and data are available on request from the corresponding author, Qing Bao (baoqing@mail.iap.ac.cn).

Author contributions

Qing Bao led the development of CAS FGOALS-f3 and all other co-authors contributed to it. Jinxiao Li participated in the development of CAS FGOALS-f3 and evaluated the simulation performance of tropical cyclones in FGOALS-f3. Yimin Liu, Lei Wang, Jing Yang, Guoxiong Wu, Xiaofei Wu, Bian He, Xiaocong Wang, Xiaoqi Zhang, Yaoxian Yang, and Zili Shen contributed to the writing of this paper.

Competing interests

The authors declare that they have no conflicts of interest.

Acknowledgments

This work was jointly funded by the Strategic Priority Research Program of the Chinese Academy of Sciences [grant number XDB40030205], the National Natural Science Foundation of China [grant numbers 42005117] and the Key Special Project for Introduced Talents Team of Southern Marine Science and Engineering Guangdong Laboratory (Guangdong) [grant numbers GML2019ZD0601].

References

Benfield, A.: Global economic losses. Weather, climate & catastrophe insight—2017 annual report. Aon Benfield UCL Hazard Research Centre Rep., 2–5, http:// thoughtleadership.aonbenfield.com/Documents/20180124-abif-annual-report-weather-climate-2017.pdf, 2018.

Bao, Q., Lin, P., Zhou, T., Liu, Y., Yu, Y., Wu, G., He, B., He, J., Li, L., and Li, J.: The flexible global ocean-atmosphere-land system model, spectral version 2: FGOALS-s2, Adv. Atmos. Sci., 30, 561-576, https://doi.org/10.1007/s00376-012-2113-9, 2013.

Bao, Q., Wu, G., Liu, Y., Yang, J., Wang, Z., and Zhou, T.: An introduction to the coupled model FGOALS1. 1-s and its performance in East Asia, Adv. Atmos. Sci., 27, 1131-1142, https://doi.org/10.1007/s00376-010-9177-1, 2010.

Bao, Q., Wu, X., Li, J., Wang, L., He, B., Wang, X., Liu, Y., and Wu, G.: Outlook for El Niño and the Indian Ocean Dipole in autumn-winter 2018–2019, Chinese Sci. Bull., 64, 73-78, 2018.

Bao, Q. and Li, J.: Progress in climate modeling of precipitation over the Tibetan Plateau, Natl. Sci. Rev., 7, 486-487, https://doi.org/10.1093/nsr/nwaa006, 2020.

Boucher, O., Servonnat, J., Albright, A. L., et al.: Presentation and evaluation of the IPSL-CM6A-LR climate model, J. Adv. Model. Earth Sy., 2020, 12, e2019MS002010, https://doi.org/10.1029/2019MS002010, 2020.

Bell, G. and Chelliah, M.: The 1999 North Atlantic and eastern North Pacific hurricane season [in "Climate Assessment for 1999"], B. Am. Meteorol. Soc., 81, S19-S22, https://doi.org/10.1175/1520-0477-80.5s.S1, 2000.

Bell, R., Hodges, K., Vidale, P. L., Strachan, J., and Roberts, M.: Simulation of the global ENSO–tropical cyclone teleconnection by a high-resolution coupled general circulation model, J. Climate, 27, 6404-6422, https://doi.org/10.1175/JCLI-D-13-00559.1, 2014.

Bengtsson, L., Böttger, H., and Kanamitsu, M.: Simulation of hurricane-type vortices in a general circulation model, Tellus, 34, 440-457, https://doi.org/10.1111/j.2153-3490.1982.tb01833.x, 1982.

Bacmeister, J. T., Wehner, M. F., Neale, R. B., Gettelman, A., Hannay, C., Lauritzen P. H., Caron, J. M., and Truesdale, J. E.: Exploratory high-resolution climate simulations using the Community Atmosphere Model (CAM), J. Climate, 27, 3073-3099, https://doi.org/10.1175/JCLI-D-13-00387.1, 2014.

Balaguru, K., Leung, L. R., Van Roekel, L. P., Golaz, J. C., Ullrich, P. A., Caldwell, P. M., Hagos, S. M., Harrop, B. E., and Mametjanov, A.: Characterizing tropical cyclones in the energy exascale earth system model Version 1, J. Adv. Model. Earth Sy., 12, e2019MS002024, https://doi.org/10.1029/2019MS002024, 2020.

Camargo, S. J., Emanuel, K. A., and Sobel, A. H.: Use of a genesis potential index to diagnose ENSO effects on tropical cyclone genesis, J. Climate, 20, 4819-4834, https://doi.org/10.1175/JCLI4282.1, 2007.

Camargo, S. J., and Sobel, A. H.: Western North Pacific tropical cyclone intensity and ENSO, J. Climate, 18.15, 2996-3006, https://doi.org/10.1175/JCLI3457.1, 2005.

Camargo, S. J.: Global and regional aspects of tropical cyclone activity in the CMIP5 models, J. Climate, 26, 9880-9902, https://doi.org/10.1175/JCLI-D-12-00549.1, 2013.

Camargo, S. J., Robertson, A. W., Barnston, A. G., and Ghil, M.: Clustering of eastern North Pacific tropical cyclone tracks: ENSO and MJO effects, Geochem. Geophy. Geosy., 9, https://doi.org/10.1029/2007GC001861, 2008.

Camargo, S. J., Wheeler, M. C., and Sobel, A. H.: Diagnosis of the MJO modulation of tropical cyclogenesis using an empirical index, J. Atmos. Sci., 66, 3061-3074, https://doi.org/10.1175/2009JAS3101.1, 2009.

Camargo, S. J. and Wing, A. A.: Tropical cyclones in climate models, Wires. Clim. Change, 7, 211-237, https://doi.org/10.1002/wcc.373, 2016.

Camp, J., Roberts, M. J., Comer, R. E., Wu, P., MacLachlan, C., Bett, P. E., Golding, N., Toumi, R., and Chan, J. C.: The western Pacific subtropical high and tropical cyclone landfall: Seasonal forecasts using the Met Office GloSea5 system, Q. J. Roy. Meteor. Soc., 145, 105-116, https://doi.org/10.1002/qj.3407, 2019.

Chen, S., Knaff, J. A., and Marks, F. D.: Effects of vertical wind shear and storm motion on tropical cyclone rainfall asymmetries deduced from TRMM, Mon. Weather Rev., 134.11, 3190-3208, https://doi.org/10.1175/MWR3245.1, 2006.

Chen, J.-H. and Lin, S.-J.: Seasonal predictions of tropical cyclones using a 25-km-resolution general circulation model, J. Climate, 26, 380-398, https://doi.org/10.1175/JCLI-D-12-00061.1, 2013.

Chutia, L., Pathak, B., Parottil, A., and Bhuyan, P. K.: Impact of microphysics parameterizations and horizontal resolutions on simulation of "MORA" tropical cyclone over Bay of Bengal using Numerical Weather Prediction Model, Meteorol. Atmos. Phys., 131, 1483-1495, https://doi.org/10.1007/s00703-018-0651-0, 2019.

设置了格式: 字体: 10 磅, 字体颜色: 自动设置, 英语(美国)

设置了格式: 字体: 10 磅, 字体颜色: 自动设置, 英语(美国)

带格式的: 缩进: 左侧: 0 厘米, 悬挂缩进: 2 字符

设置了格式: 字体颜色: 自动设置, 英语(美国)

设置了格式: 字体颜色: 自动设置, 英语(美国)

设置了格式: 字体: 10 磅, 字体颜色: 自动设置, 英语(美国)

设置了格式: 字体颜色: 自动设置, 英语(美国)

设置了格式: 字体: 10 磅, 字体颜色: 自动设置, 英语(美国)

设置了格式: 字体颜色: 自动设置, 英语(美国)

设置了格式: 字体: 10 磅, 字体颜色: 自动设置, 英语(美国)

设置了格式: 字体颜色: 自动设置, 英语(美国)

设置了格式: 字体: 10 磅, 字体颜色: 自动设置, 英语(美国)

设置了格式: 字体颜色: 自动设置, 英语(美国)

设置了格式: 字体: 10 磅, 字体颜色: 自动设置, 英语(美国)

设置了格式: 字体颜色: 自动设置, 英语(美国)

设置了格式: 字体: 10 磅, 字体颜色: 自动设置, 英语(美国)

设置了格式: 字体颜色: 自动设置, 英语(美国)

设置了格式: 字体: 10 磅, 字体颜色: 自动设置, 英语(美国)

设置了格式: 字体颜色: 自动设置, 英语(美国)

设置了格式: 字体: 10 磅, 字体颜色: 自动设置, 英语(美国)

设置了格式: 字体颜色: 自动设置, 英语(美国)

设置了格式: 字体颜色: 自动设置

设置了格式: 字体: 10 磅, 字体颜色: 自动设置, 英语(美国)

域代码已更改

设置了格式: 超链接, 字体: 10 磅, 字体颜色: 自动设置, 英语(美国)

删除了: Balaguru, K., Foltz, G. R., Leung, L., R., Kaplan, J., Xu, W., Reul, N., and Chapron, B. et al.: Pronounced impact of salinity on rapidly intensifying tropical cyclones, Bull. Am. Meteorol. Soc., 101.9, E1497-E1511, https://doi.org/10.1175/BAMS-D-19-0303.1, 2020.…

Craig, A. P., Vertenstein, M., and Jacob, R.: A new flexible coupler for earth system modeling developed for CCSM4 and CESM1, Int. J. High Perform. C., 26, 31-42, https://doi.org/10.1177/1094342011428141, 2012.

Clough, S., Shephard, M., Mlawer, E., Delamere, J., Iacono, M., Cady-Pereira, K., Boukabara, S., and Brown, P.: Atmospheric radiative transfer modeling: a summary of the AER codes, J. Quant. Spectrosc. RA., 91, 233-244, https://doi.org/10.1016/j.jqsrt.2004.05.058, 2005.

Dee, D. P., Uppala, S., Simmons, A., Berrisford, P., Poli, P., Kobayashi, S., Andrae, U., Balmaseda, M., Balsamo, G., and Bauer, d. P.: The ERA-Interim reanalysis: Configuration and performance of the data assimilation system, Q. J. Roy. Meteor. Soc., 137, 553-597, https://doi.org/10.1002/qj.828, 2011.

Delworth, T. L., Cooke, W. F., Adcroft, A., Bushuk, M., Chen, J. H., Dunne, K. A., Ginoux, P., Gudgel, R., Hallberg, R. W., and Harris, L.: SPEAR: The Next Generation GFDL Modeling System for Seasonal to Multidecadal Prediction and Projection, J. Adv. Model. Earth Sy., 12, e2019MS001895, https://doi.org/10.1029/2019MS001895, 2020.

Emanuel, K.: Downscaling CMIP5 climate models shows increased tropical cyclone activity over the 21st century, P. Natl. Acad. Sci. USA., 110, 12219-12224, https://doi.org/10.1073/pnas.1301293110 2013.

Emanuel, K.: Assessing the present and future probability of Hurricane Harvey's rainfall, P. Natl. Acad. Sci. USA., 114, 12681-12684, https://doi.org/10.1073/pnas.1716222114, 2017.

Emanuel, K., DesAutels, C., Holloway, C., and Korty, R.: Environmental control of tropical cyclone intensity, J. Atmos. Sci., 61, 843-858, https://doi.org/10.1175/1520-0469(2004)061<0843:ECOTCI>2.0.CO;2, 2004.

Emanuel, K.: Sensitivity of tropical cyclones to surface exchange coefficients and a revised steady-state model incorporating eye dynamics, J. Atmos. Sci., 52, 3969-3976, https://doi.org/10.1175/1520-0469(1995)052<3969:SOTCTS>2.0.CO;2, 1995.

Emanuel, K., and Sobel, A.: Response of tropical sea surface temperature, precipitation, and tropical cyclone-related variables to changes in global and local forcing, J. Adv. Model. Earth Sy., 5, 447-458, https://doi.org/10.1002/jame.20032, 2013.

Eyring, V., Bony, S., Meehl, G. A., Senior, C. A., Stevens, B., Stouffer, R. J., and Taylor, K. E.: Overview of the Coupled Model Intercomparison Project Phase 6 (CMIP6) experimental design and organization, Geosci. Model Dev., 9, https://doi.org/10.5194/gmd-9-1937-2016, 2016.

Gray, W. M.: Global view of the origin of tropical disturbances and storm, Monthly Weather Review, 96(10), 669-700, https://doi.org/10.1175/1520-0493(1968)096<0669:GVOTOO>2.0.CO;2, 1968.

Gray, W. M.: Atlantic seasonal hurricane frequency. Part I: El Niño and 30 mb quasi-biennial oscillation influences, Mon. Weather Rev., 112.9, 1649-1668, https://doi.org/10.1175/1520-0493(1984)112<1649:ASHFPI>2.0.CO;2, 1984.

Gutjahr, O., Putrasahan, D., Lohmann, K., Jungclaus, J. H., von Storch, J. S., Brüggemann, N., Haak, H., and Stössel, A.: Max Planck Institute Earth System Model (MPI-ESM1.2) for High-Resolution Model Intercomparison Project (HighResMIP), Geosci. Model Dev., 12, 3241-3281, doi:10.5194/gmd-12-3241-2019, 2019.

Haarsma, R. J., Mitchell, J. F., and Senior, C.: Tropical disturbances in a GCM, Clim. Dynam., 8, 247-257, https://doi.org/10.1007/BF00198619, 1993.

Haarsma, R. J., Roberts, M. J., Vidale, P. L., Senior, C. A., Bellucci, A., Bao, Q., Chang, P., Corti, S., Fučkar, N. S., and Guemas, V.: High resolution model intercomparison project (HighResMIP v1. 0) for CMIP6, Geosci. Model Dev., 9, 4185-4208, https://doi.org/10.5194/gmd-9-4185-2016, 2016.

Haarsma, R., Acosta, M., Bakhshi, R., et al.: HighResMIP versions of EC-Earth: EC-Earth3P and EC-Earth3P-HR–description, model computational performance and basic validation, Geosci. Model Dev., 13, 3507-3527, https://doi.org/10.5194/gmd-13-3507-2020, 2020.

Hall, J. D., Matthews, A. J., and Karoly, D. J.: The modulation of tropical cyclone activity in the Australian region by the Madden–Julian oscillation, Mon. Weather Rev., 129, 2970-2982, https://doi.org/10.1175/1520-0493(2001)129<2970:TMOTCA>2.0.CO;2, 2001.

He, B., Bao, Q., Wang, X., Zhou, L., Wu, X., Liu, Y., Wu, G., Chen, K., He, S., Hu, W., Li, J., Li, J., Nian, G., Wang, L., Yang, J., Zhang, M., and Zhang, X.: CAS FGOALS-f3-L model datasets for CMIP6 historical atmospheric model Intercomparison project simulation, Adv. Atmos. Sci., 36, 771-778, https://doi.org/10.1007/s00376-019-9027-8, 2019..

He, B., Liu, Y., Wu, G., Bao, Q., Zhou, T., Wu, X., Wang, L., Li, J., Wang, X., and Li, J.: CAS FGOALS-f3-L Model Datasets for CMIP6 GMMIP Tier-1 and Tier-3 Experiments, Adv. Atmos. Sci., 37, 18-28, https://doi.org/10.1007/s00376-019-9085-y, 2020.

Hou, A. Y., Kakar, R. K., Neeck, S., Azarbarzin, A. A., Kummerow, C. D., Kojima, M., Oki, R., Nakamura, K., and Iguchi, T.: The global precipitation measurement mission, B. Am. Meteorol. Soc., 95, 701-722, https://doi.org/10.1175/BAMS-D-13-00164.1, 2014.

Hodges, K., Cobb, A., and Vidale, P. L.: How well are tropical cyclones represented in reanalysis datasets?, J. Climate, 30.14, 5243-5264, https://doi.org/10.1175/JCLI-D-16-0557.1, 2017.

Hunke, E., Lipscomb, W., Turner, A., Jeffery, N., and Elliott, S.: CICE: The los alamos sea ice model documentation and software user's manual, version 4.1, 2010.

Hunke, E. C., Lipscomb, W. H., Turner, A., Jeffery, N., and Elliott, S.: CICE: the Los Alamos sea ice model documentation and software user's manual, T-3 Fluid Dynamics Group, Los Alamos National Laboratory, Los Alamos, NM, 87545, 2008.

Harris, L. M. and Lin, S.-J.: Global-to-regional nested grid climate simulations in the GFDL high resolution atmospheric model, J. Climate, 27, 4890-4910, https://doi.org/10.1175/JCLI-D-13-00596.1, 2014.

Klotzbach, P. J.: The Madden–Julian oscillation's impacts on worldwide tropical cyclone activity, J. Climate, 27, 2317-2330, https://doi.org/10.1175/JCLI-D-13-00483.1, 2014.

Kim, H., M., Webster, P. J., and Curry, J. A.: Modulation of North Pacific tropical cyclone activity by three phases of ENSO, J. Climate, 24.6, 1839-1849, https://doi.org/10.1175/2010JCLI3939.1, 2011.

Kim, H. S., Vecchi, G. A., Knutson, T. R., Anderson, W. G., Delworth, T. L., Rosati, A., Zeng, F., and Zhao, M.: Tropical cyclone simulation and response to CO_2 doubling in the GFDL CM2. 5 high-resolution coupled climate model, J. Climate, 27.21, 8034-8054, https://doi.org/10.1175/JCLI-D-13-00475.1, 2014.

Kim, D., Ho, C. H., Park, D. S., Chan, J. C. L., Jung, Y.: The Relationship between Tropical Cyclone Rainfall Area and Environmental Conditions over the Subtropical Oceans, J. Climate, 31(12), 4605-4616, https://doi.org/10.1175/JCLI-D-17-0712.1, 2018.

Knapp, K. R., Kruk, M. C., Levinson, D. H., Diamond, H. J., and Neumann, C. J.: The international best track archive for climate stewardship (IBTrACS) unifying tropical cyclone data, B. Am. Meteorol. Soc., 91, 363-376, https://doi.org/10.1175/2009BAMS2755.1, 2010.

Knutson, T., Camargo, S. J., Chan, J. C., Emanuel, K., Ho, C.-H., Kossin, J., Mohapatra, M., Satoh, M., Sugi, M., and Walsh, K.: Tropical Cyclones and Climate Change Assessment: Part I: Detection and Attribution, B. Am. Meteorol. Soc., 100, 1987-2007, https://doi.org/10.1175/BAMS-D-18-0189.1, 2019.

Knutson, T., Camargo, S. J., Chan, J. C., Emanuel, K., Ho, C.-H., Kossin, J., Mohapatra, M., Satoh, M., Sugi, M., and Walsh, K.: Tropical cyclones and climate change assessment: Part II: Projected response to anthropogenic warming, B. Am. Meteorol. Soc., 101, E303-E322, https://doi.org/10.1175/BAMS-D-18-0194.1, 2020.

Knutson, T. R., Manabe, S., and Gu, D.: Simulated ENSO in a global coupled ocean–atmosphere model: Multidecadal amplitude modulation and CO_2 sensitivity, J. Climate, 10, 138-161, https://doi.org/10.1175/1520-0442(1997)010<0138:SEIAGC>2.0.CO;2, 1997.

Knutson, T. R., Sirutis, J. J., Garner, S. T., Held, I. M., and Tuleya, R. E.: Simulation of the recent multidecadal increase of Atlantic hurricane activity using an 18-km-grid regional model, B. Am. Meteorol. Soc., 88, 1549-1565, https://doi.org/10.1175/BAMS-88-10-1549, 2007.

Krishnamurthy, L., Vecchi, G. A., Msadek, R., Murakami, H., Wittenberg, A., and Zeng, F.: Impact of strong ENSO on regional tropical cyclone activity in a high-resolution climate model in the North Pacific and North Atlantic Oceans, J. Climate, 29, 2375-2394, https://doi.org/10.1175/JCLI-D-15-0468.1, 2016.

Krishnamurti, T. N. and Oosterhof, D.: Prediction of the life cycle of a supertyphoon with a high-resolution global model, B. Am. Meteorol. Soc., 70, 1218-1230, https://doi.org/10.1175/1520-0477(1989)070<1218:POTLCO>2.0.CO;2, 1989.

Larson, S. and Kirtman, B.: The Pacific Meridional Mode as a trigger for ENSO in a high-resolution coupled model, B. Am. Meteorol. Soc. B. Am. Meteorol. Soc., 40, 3189-3194, https://doi.org/10.1002/grl.50571, 2013.

Lawrence, D. M., Oleson, K. W., Flanner, M. G., Thornton, P. E., Swenson, S. C., Lawrence, P. J., Zeng, X., Yang, Z. L., Levis, S., and Sakaguchi, K.: Parameterization improvements and functional and structural advances in version 4 of the Community Land Model, J. Adv. Model. Earth Sy., 3, https://doi.org/10.1029/2011MS00045, 2011.

Li, H. and Ryan L. S.: Tropical cyclone activity in the high-resolution community earth system model and the impact of ocean coupling, J. Adv. Model. Earth Sy. 10.1, 165-186, https://doi.org/10.1002/2017MS001199, 2018.

Li, J., Bao, Q., Liu, Y., Wu, G., Wang, L., He, B., Wang, X., and Li, J.: Evaluation of FAMIL2 in simulating the climatology and seasonal-to-interannual variability of tropical cyclone characteristics, J. Adv. Model. Earth Sy., 11, 1117-1136, https://doi.org/10.1029/2018MS001506, 2019.

Li, J., Bao, Q., Liu, Y., and Wu, G.: Evaluation of the computational performance of the finite-volume atmospheric model of the IAP/LASG (FAMIL) on a high-performance computer, Atmos. Oceanic Sci. Lett., 10, 329-336, https://doi.org/10.1080/16742834.2017.1331111, 2017.

Lim, Y. K., Schubert, S. D., Reale, O., Lee, M, I., Molod, A. M., and Suarez, M. J.: Sensitivity of tropical cyclones to parameterized convection in the NASA GEOS-5 mode, J. Climate, 28, 551-573, https://doi.org/10.1175/JCLI-D-14-00104.1, 2015.

Liebmann, B., Hendon, H. H., and Glick, J. D.: The relationship between tropical cyclones of the western Pacific and Indian Oceans and the Madden-Julian oscillation, J. Meteorol. Soc. Jpn., 72, 401-412, https://doi.org/10.2151/jmsj1965.72.3_401, 1994.

Lin, S.-J.: A "vertically Lagrangian" finite-volume dynamical core for global models, Mon. Weather Rev., 132, 2293-2307, https://doi.org/10.1175/1520-0493(2004)132<2293:AVLFDC>2.0.CO;2, 2004.

Lin, Y.-L., Farley, R. D., and Orville, H. D.: Bulk parameterization of the snow field in a cloud model, J. Clim. Appl. Meteorol., 22, 1065-1092, https://doi.org/10.1175/1520-0450(1983)022<1065:BPOTSF>2.0.CO;2, 1983.

Liu, H., Lin, P., Yu, Y., and Zhang, X.: The baseline evaluation of LASG/IAP climate system ocean model (LICOM) version 2, Acta Meteorol. Sin., 26, 318-329, https://doi.org/10.1007/s13351-012-0305-y, 2012.

Manabe, S. and Broccoli, A.: Mountains and arid climates of middle latitudes, Science, 247, 192-195, https://doi.org/10.1126/science.247.4939.192, 1990.

Manabe, S., Holloway Jr, J. L., and Stone, H. M.: Tropical circulation in a time-integration of a global model of the atmosphere, J. Atmos. Sci., 27, 580-613, https://doi.org/10.1175/1520-0469(1970)027<0580:TCIATI>2.0.CO;2, 1970.

Manganello, J. V., Hodges, K. I., Cash, B. A., Kinter III, J. L., Altshuler, E. L., Fennessy, M. J., Vitart, F., Molteni, F., and Towers, P.: Seasonal forecasts of tropical cyclone activity in a high-atmospheric-resolution coupled prediction system, J. Climate, 29, 1179-1200, https://doi.org/10.1175/JCLI-D-15-0531.1 , 2016.

Manganello, J. V., Hodges, K. I., Kinter III, J. L., Cash, B. A., Marx, L., Jung, T., Achuthavarier, D., Adams, J. M., Altshuler, E. L., and Huang, B.: Tropical cyclone climatology in a 10-km global atmospheric GCM: toward weather-resolving climate modeling, J. Climate, 25, 3867-3893, https://doi.org/10.1175/JCLI-D-11-00346.1, 2012.

Masson, S., Terray, P., Madec, G., Luo, J.-J., Yamagata, T., and Takahashi, K.: Impact of intra-daily SST variability on ENSO characteristics in a coupled model, Clim. Dynam., 39, 681-707, https://doi.org/10.1007/s00382-011-1247-2, 2012.

Matsuura, T., Yumoto, M., Iizuka, S., and Kawamura, R.: Typhoon and ENSO simulation using a high-resolution coupled GCM, Geophys. Res. Lett., 26, 1755-1758, https://doi.org/10.1029/1999GL900329, 1999.

Meehl, G. A., Shields, C., Arblaster, J. M., Annamalai, H., and Neale, R.: Intraseasonal, seasonal, and interannual characteristics of regional monsoon simulations in CESM2, J. Adv. Model. Earth Sy., 2020. e2019MS001962, https://doi.org/10.1029/2019MS001962, 2020.

Mendelsohn, R., Emanuel, K., Chonabayashi, S., and Bakkensen, L.: The impact of climate change on global tropical cyclone damage, Nat. Clim. Change, 2, 205-209, https://doi.org/10.1038/nclimate1357, 2012.

Murakami, H., Sugi, M., and Kitoh, A.: Future changes in tropical cyclone activity in the North Indian Ocean projected by high-resolution MRI-AGCMs, Clim. Dynam., 40, 1949-1968, https://doi.org/10.1007/s00382-012-1407-z, 2013.

Murakami, H., Vecchi, G. A., Villarini, G., Delworth, T. L., Gudgel, R., Underwood, S., Yang, X., Zhang, W., and Lin, S.-J.: Seasonal forecasts of major hurricanes and landfalling tropical cyclones using a high-resolution GFDL coupled climate model, J. Climate, 29, 7977-7989, https://doi.org/10.1175/JCLI-D-16-0233.1, 2016.

Murakami, H., Wang, Y., Yoshimura, H., Mizuta, R., Sugi, M., Shindo, E., Adachi, Y., Yukimoto, S., Hosaka, M., and Kusunoki, S.: Future changes in tropical cyclone activity projected by the new high-resolution MRI-AGCM, J. Climate, 25, 3237-3260, https://doi.org/10.1007/s00382-012-1407-z, 2012.

Mizuta, R., Yoshimura, H., Murakami, H., Matsueda, M., Endo, H., Ose, T., Kamiguchi, K., Hosaka, M., Sugi, M., Yukimoto, S., Kusunoki, S., and Kitoh, A.: Climate simulations using MRI-AGCM3. 2 with 20-km grid, J. Meteorol. Soc. Jpn., 90, 233-258, https://doi.org/10.2151/jmsj.2012-A12, 2012.

Müller, W. A., Jungclaus, J. H., Mauritsen, T., Mauritsen, T., Baehr, J., Bittner, M., Budich, R., Bunzel, F., Esch, M., Ghosh, R., Haak, H., Ilyina, T., Kleine, T., Kornblueh, L., Li, H., Modali, K., Notz, D., Pohlmann, H., Roeckner, E., Stemmler, I., Tian, F., and Marotzke, J.: A Higher-resolution Version of the Max Planck Institute Earth System Model (MPI-ESM1. 2-HR). J. Adv. Model. Earth Sy., 10, 1383-1413, https://doi.org/10.1029/2017MS001217, 2018.

Ma, Y., Davidson, N. E., Xiao, Y., and Bao, J. W.: Revised parameterization of air–sea exchanges in high winds for operational numerical prediction: Impact on tropical cyclone track, intensity, and rapid intensification, Weather Forecast., 32, 821-848, https://doi.org/10.1175/WAF-D-15-0109.1, 2017.

Oleson, K. W., Lawrence, D. M., Gordon, B., Flanner, M. G., Kluzek, E., Peter, J., Levis, S., Swenson, S. C., Thornton, E., and Feddema, J.: Technical description of version 4.0 of the Community Land Model (CLM), 2010.

Oouchi, K., Yoshimura, J., Yoshimura, H., Mizuta, R., Kusunoki, S., and Noda, A.: Tropical cyclone climatology in a global-warming climate as simulated in a 20 km-mesh global atmospheric model: Frequency and wind intensity analyses, J. Meteorol. Soc. Jpn., 84, 259-276, https://doi.org/10.2151/jmsj.84.259, 2006.

Philander, S., Pacanowski, R., Lau, N.-C., and Nath, M.: Simulation of ENSO with a global atmospheric GCM coupled to a high-resolution, tropical Pacific Ocean GCM, J. Climate, 5, 308-329, https://doi.org/10.1175/1520-0442(1992)005<0308:SOEWAG>2.0.CO;2, 1992.

Putman, W. M. and Lin, S.-J.: Finite-volume transport on various cubed-sphere grids, J. Comput. Phys., 227, 55-78, https://doi.org/10.1016/j.jcp.2007.07.022, 2007.

Park, S. and Bretherton, C. S.: The University of Washington shallow convection and moist turbulence schemes and their impact on climate simulations with the Community Atmosphere Model, J. Climate, 22, 3449-3469, https://doi.org/10.1175/2008JCLI2557.1, 2009.

Palmer, T., Shutts, G., and Swinbank, R.: Alleviation of a systematic westerly bias in general circulation and numerical weather prediction models through an orographic gravity wave drag parametrization, Q. J. Roy. Meteor. Soc., 112, 1001-1039, https://doi.org/10.1002/qj.49711247406, 1986.

Roberts, M. J., Camp, J., Seddon, J., Vidale, P. L., Hodges, K., Vanniere, B., Mecking, J., Haarsma, R., Bellucci, A., and Scoccimarro, E.: Impact of Model Resolution on Tropical Cyclone Simulation Using the HighResMIP–PRIMAVERA Multimodel Ensemble, J. Climate, 33, 2557-2583, https://doi.org/10.1175/JCLI-D-19-0639.1, 2020.

Roberts, C. D., Senan, R., Molteni, F., Boussetta, S., Mayer, M., and Keeley, S.: Climate model configurations of the ECMWF integrated forecast system (ECMWF-IFS cycle 43r1) for HighResMIP, Geosci. Model Dev., 11, 3681–3712, https://doi.org/10.5194/gmd-11-3681-2018, 2018.

Schneider, E. K., Kirtman, B. P., DeWitt, D. G., Rosati, A., Ji, L., and Tribbia, J. J.: Retrospective ENSO forecasts: sensitivity to atmospheric model and ocean resolution, Mon. Weather Rev., 131, 3038-3060, https://doi.org/10.1175/1520-0493(2003)131<3038:REFSTA>2.0.CO;2, 2003.

Simpson, R. H. and Saffir, H.: The hurricane disaster potential scale, Weatherwise, 27, 169, 1974.

Strachan, J., Vidale, P. L., Hodges, K., Roberts, M., and Demory, M.-E.: Investigating global tropical cyclone activity with a hierarchy of AGCMs: The role of model resolution, J. Climate, 26, 133-152, https://doi.org/10.1175/JCLI-D-12-00012.1, 2013.

Sakradzija, M., Seifert, A., Dipankar, A.: A stochastic scale-aware parameterization of shallow cumulus convection across the convective gray zone, J. Adv. Model. Earth Sy., 8, 786-812, https://doi.org/10.1002/2016MS000634, 2016.

Small, R. J, Bacmeister, J., Bailey, D., Baker, D., Bishop, S., Bryan, F., et al.: A new synoptic scale resolving global climate simulation using the Community Earth System Model, J. Adv. Model. Earth Sy, 6.4, 1065-1094, https://doi.org/10.1002/2014MS000363, 2014.

Scoccimarro, E., Fogli, P. G., Reed, K. A., Gualdi, S., Masina, S., and Navarra, A.: Tropical cyclone interaction with the ocean: The role of high-frequency (subdaily) coupled processes, J. Climate, 30.1, 145-162, https://doi.org/10.1175/JCLI-D-16-0292.1, 2017.

Ullrich, P. A., Zarzycki, C. M., McClenny, E. E., Pinheiro, M. C., Stansfield, A. M., and Reed, K. A.: TempestExtremes v2.1: A Community Framework for Feature Detection, Tracking and Analysis in Large Datasets, Geosci. Model Dev. Discuss. [preprint], https://doi.org/10.5194/gmd-2020-303, in review, 2021.

Ullrich, P. A. and Zarzycki, C. M.: TempestExtremes: a framework for scale-insensitive pointwise feature tracking on unstructured grids, Geosci. Model Dev., 10, 1069–1090, https://doi.org/10.5194/gmd-10-1069-2017, 2017.

Vitart, F., Ardilouze, C., Bonet, A., Brookshaw, A., Chen, M., Codorean, C., Déqué, M., Ferranti, L., Fucile, E., and Fuentes, M.: The subseasonal to seasonal (S2S) prediction project database, B. Am. Meteorol. Soc., 98, 163-173, https://doi.org/10.1175/BAMS-D-16-0017.1, 2017.

Vitart, F. and Robertson, A. W.: The sub-seasonal to seasonal prediction project (S2S) and the prediction of extreme events, Npj Clim. Atmos. Sci., 1, 3, https://doi.org/10.1038/s41612-018-0013-0, 2018.

Voosen, P.: The weather master. American Association for the Advancement of Science, 2017.

Voldoire, A., Saint-Martin, D., Sénési, S., et al.: Evaluation of CMIP6 deck experiments with CNRM-CM6-1. J. Adv. Model. Earth Sy., 11, 2177-2213, https://doi.org/10.1029/2019MS001683., 2019.

Walsh, K., Fiorino, M., Landsea, C., and McInnes, K.: Objectively determined resolution-dependent threshold criteria for the detection of tropical cyclones in climate models and reanalyses, J. Climate, 20, 2307-2314, https://doi.org/10.1175/JCLI4074.1, 2007.

Walsh, K., Lavender, S., Scoccimarro, E., and Murakami, H.: Resolution dependence of tropical cyclone formation in CMIP3 and finer resolution models, Clim. Dynam., 40, 585-599, https://doi.org/10.1007/s00382-012-1298-z, 2013.

Walsh, K. J., Camargo, S. J., Vecchi, G. A., Daloz, A. S., Elsner, J., Emanuel, K., Horn, M., Lim, Y.-K., Roberts, M., and Patricola, C.: Hurricanes and climate: the US CLIVAR working group on hurricanes, B. Am. Meteorol. Soc., 96, 997-1017, https://doi.org/10.1175/BAMS-D-13-00242.1, 2015.

Walsh, K. J., McBride, J. L., Klotzbach, P. J., Balachandran, S., Camargo, S. J., Holland, G., Knutson, T. R., Kossin, J. P., Lee, T. C., and Sobel, A.: Tropical cyclones and climate change, Wires. Clim. Change, 7, 65-89, https://doi.org/10.1002/wcc.371, 2016.

Williams, K. D., Copsey, D., Blockley, E. W., et al.: The Met Office global coupled model 3.0 and 3.1 (GC3. 0 and GC3. 1) configurations, J. Adv. Model. Earth Sy., 10, 357-380, https://doi.org/10.1002/2017MS001115, 2018.

Wong, M. L. M., Chan, J. C. L.: Tropical cyclone intensity in vertical wind shear, J. Atmos. Sci, 61(15), 1859-1876, https://doi.org/10.1175/1520-0469(2004)061<1859:TCIIVW>2.0.CO;2, 2004.

Wu, G. and Lau, N.-C.: A GCM simulation of the relationship between tropical-storm formation and ENSO, Mon. Weather Rev., 120, 958-977, https://doi.org/10.1175/1520-0493(1992)120<0958:AGSOTR>2.0.CO;2, 1992.

Wu, G., Liu, H., Zhao, Y., and Li, W.: A nine-layer atmospheric general circulation model and its performance, Adv. Atmos. Sci., 13, 1-18, https://doi.org/10.1007/BF02657024, 1996.

Xiang, B., Lin, S.-J., Zhao, M., Zhang, S., Vecchi, G., Li, T., Jiang, X., Harris, L., and Chen, J.-H.: Beyond weather time-scale prediction for Hurricane Sandy and Super Typhoon Haiyan in a global climate model, Mon. Weather Rev., 143, 524-535, https://doi.org/10.1175/MWR-D-14-00227.1, 2015.

Xu, K.-M. and Randall, D. A.: A semiempirical cloudiness parameterization for use in climate models, J. Atmos. Sci., 53, 3084-3102, https://doi.org/10.1175/1520-0469(1996)053<3084:ASCPFU>2.0.CO;2, 1996.

Ying, M., Zhang, W., Yu, H., Lu, X., Feng, J., Fan, Y., Zhu, Y., and Chen, D.: An overview of the China Meteorological Administration tropical cyclone database, J. Atmos. Ocean. Tech., 31, 287-301, https://doi.org/10.1175/JTECH-D-12-00119.1, 2014.

Yu, Y., Tang, S., Liu, H., Lin, P., and Li, X.: Development and evaluation of the dynamic framework of an ocean general circulation model with arbitrary orthogonal curvilinear coordinate, Chinese Journal of Atmospheric Sciences, 42, 877–889, https://doi.org/10.3878/j.issn.1006-9895.1805. 17284, 2018.

Zarzycki, C. M. and Jablonowski, C.: Experimental tropical cyclone forecasts using a variable-resolution global model, Mon. Weather Rev., 143, 4012-4037, https://doi.org/10.1175/MWR-D-15-0159.1, 2015.

Zhang, C.: Madden–Julian oscillation: Bridging weather and climate, B. Am. Meteorol. Soc., 94, 1849-1870, https://doi.org/10.1175/BAMS-D-12-00026.1, 2013.

Zhang, W., Vecchi, G. A., Murakami, H., Delworth, T., Wittenberg, A. T., Rosati, A., Underwood, S., Anderson, W., Harris, L., and Gudgel, R.: Improved simulation of tropical cyclone responses to ENSO in the western North Pacific in the high-resolution GFDL HiFLOR coupled climate model, J. Climate, 29, 1391-1415, https://doi.org/10.1175/JCLI-D-15-0475.1, 2016.

Zhang, J. A., Rogers, R. F., and Tallapragada, V.: Impact of parameterized boundary layer structure on tropical cyclone rapid intensification forecasts in HWRF, Mon. Weather Rev., 145, 1413-1426, https://doi.org/10.1175/MWR-D-16-0129.1, 2017.

Zhao, M., Held, I. M., Lin, S.-J., and Vecchi, G. A.: Simulations of global hurricane climatology, interannual variability, and response to global warming using a 50-km resolution GCM, J. Climate, 22, 6653-6678, https://doi.org/10.1175/2009JCLI3049.1, 2009.

Zhou, L., Bao, Q., Liu, Y., Wu, G., Wang, W. C., Wang, X., He, B., Yu, H., and Li, J.: Global energy and water balance: Characteristics from Finite-volume Atmospheric Model of the IAP/LASG (FAMIL1), J. Adv. Model. Earth Sy., 7, 1-20, https://doi.org/10.1002/2014MS000349, 2015.

Zhou, L., Lin, S. J., Chen, J. H., Harris, L. M., Chen, X., and Rees, S. L.: Toward Convective-Scale Prediction within the Next Generation Global Prediction System, B. Am. Meteorol. Soc., 100, 1225-1243, https://doi.org/10.1175/BAMS-D-17-0246.1, 2019.

Zhou, T., Turner, A. G., Kinter, J. L., Wang, B., Qian, Y., Chen, X., Wu, B., Liu, B., Zou, L., and Bian, H.: GMMIP (v1. 0) contribution to CMIP6: global monsoons model inter-comparison project, Geosci. Model Dev., 9, 3589-3604, https://doi.org/10.5194/gmd-9-3589-2016, 2016.

Table 1. Dynamical core and physics parameterization schemes used in FGOALS-f3.

Model configuration	FGOALS-f3
Dynamical core	Finite-Volume Cubed-Sphere Dynamical core
Boundary layer scheme	University of Washington Moist Turbulence parameterization (Park & Bretherton, 2009)
Radiation scheme	Rapid Radiative Transfer Model for GCMs (Clough et al., 2005)
Gravity wave drag scheme	Palmer et al. (1996)
Cloud fraction diagnosis scheme	Xu & Randall (1996)
Convection microphysics scheme	Resolving Convective Precipitation (Bao and Li, 2020)

715 **Table 2.** Comparison of resolutions, time steps and length of simulations in FGOALS-f3 for HighResMIP Tier 1.

Model configuration	100 km FGOALS-f3	25 km FGOALS-f3
Horizontal resolution	C96 (about 100 km)	C384 (about 25 km)
Number of vertical layers	32	32
Number of vertical remapping operations per physical time step with dynamical integration (k_split)	2	6
Number of small dynamic time steps between the vertical remapping operations (n_split)	6	15
Time step of dynamical core (min)	30	30
Time step of physical processes (min)	30	30
Frequency of radiative transmission (h)	1	1
Minimum time step of microphysics scheme (s)	150	150
Length of simulations	1950–2014	1950–2014

Table 3. Comparison of tropical cyclone identification criterion between FGOALS-f3-L and FGOALS-f3-H.

Variable	FGOALS-f3-L	FGOALS-f3-H
Surface wind speed threshold ($m\ s^{-1}$)*	≥14.0	≥15.4
850 hPa absolute vorticity (s^{-1})	$\geq 3.5 \times 10^{-5}$	$\geq 3.5 \times 10^{-5}$
Warm core (average temperature between 300 and 500 hPa (℃)	≥1	≥1
Lifetime (h)	≥72	≥72

* The criteria for the surface wind speed were corrected between FGOALS-f3-L and FGOALS-f3-H (Walsh et al., 2007).

720 **Table 4.** Observed and simulated average tropical cyclone number, both globally and by ocean basin, in the northern Indian (NI), western Pacific (WP), eastern Pacific (EP), northern Atlantic (NA), southern Indian Ocean (SI), southern Pacific (SP) and southern Atlantic (SA) oceans.

Data source	Global	NI	WP	EP	NA	SI	SP	SA
IBTrACS	82.67	4.05	26.24	15.00	13.85	14.25	9.14	0.14
FGOALS-f3-L	53.14	1.98	25.04	3.96	7.54	7.34	6.83	0.45
FGOALS-f3-H	67.72	3.25	27.46	10.00	11.83	8.63	6.09	0.46

Table 5. Observed and simulated averaged ACE (units: 10^4 kt) in the northern Indian (NI), western Pacific (WP), eastern Pacific (EP), northern Atlantic (NA), southern Indian (SI), and southern Pacific (SP) oceans.

Data source	NI	WP	EP	NA	SI	SP
IBTrACS	24.21	258.75	137.42	133.13	114.25	67.58
FGOALS-f3-L	12.13	170.47	7.83	69.38	50.50	60.30
FGOALS-f3-H	32.08	247.66	43.66	89.10	68.16	61.21

Table 6. Information about the GCMs participating in the HighResMIP.

Institution	Model name	Horizontal resolution/nominal resolution (km)	References
Chinese Academy of Sciences	FGOALS-f3-L	C96/100	Bao et al. (2020)
	FGOALS-f3-H	C384/25	He et al. (2019)
			Li et al. (2019)
Meteorological Research Institute	MRI-AGCM3-2-H	T319/50	Mizuta et al. (2012)
	MRI-AGCM3-2-S	T959/25	Murakami et al. (2012)
Max Planck Institute for Meteorology	MPI-ESM1-2-HR	T127/100	Müller et al. (2018) Gutjahr et al. (2019)
	MPI-ESM1-2-XR	T255/50	
Institute Pierre Simon Laplace	IPSL-CM6A-LR	N96/250	Boucher et al. (2020)
	IPSL-CM6A-ATM-HR	N256/50	
European Centre for Medium-Range Weather Forecasts	ECMWF-IFS-LR	Tco199/100	Roberts et al. (2018)
	ECMWF-IFS-HR	Tco399/25	
EC-Earth-Consortium	EC-Earth3P	T255/100	Haarsma et al. (2020)
	EC-Earth3-HR	T511/50	
Centre National de Recherches Meteorologiques	CNRM-CM6-1	T127/250	Voldoire et al. (2019)
	CNRM-CM6-1-HR	T359/50	
Met Office Hadley Centre	HadGEM3-GC31-LM	N96/250	Williams et al. (2018)
	HadGEM3-GC31-HM	N512/50	

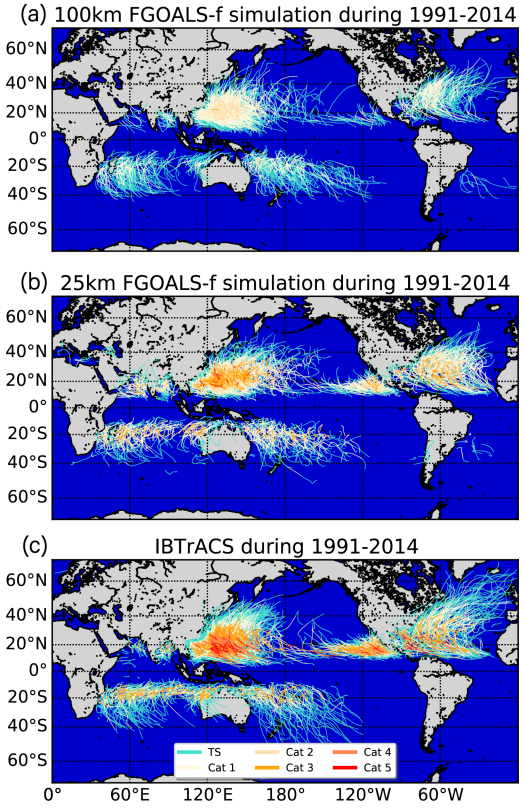

Figure 1. Global tropical cyclone tracks (lines) and intensities (colors) during the time period 1991–2014 between (a) FGOALS-f3-L, (b) FGOALS-f3-H and (c) IBTrACS. The tropical cyclones simulated by FGOALS-f3-L/H are picked out using an objective feature-tracking approach and only those tropical cyclones with a lifetime >3 days are shown. The definition of intensity threshold is consistent with the Saffir–Simpson scale: TS, tropical storm; Cat 1–5, category 1–5.

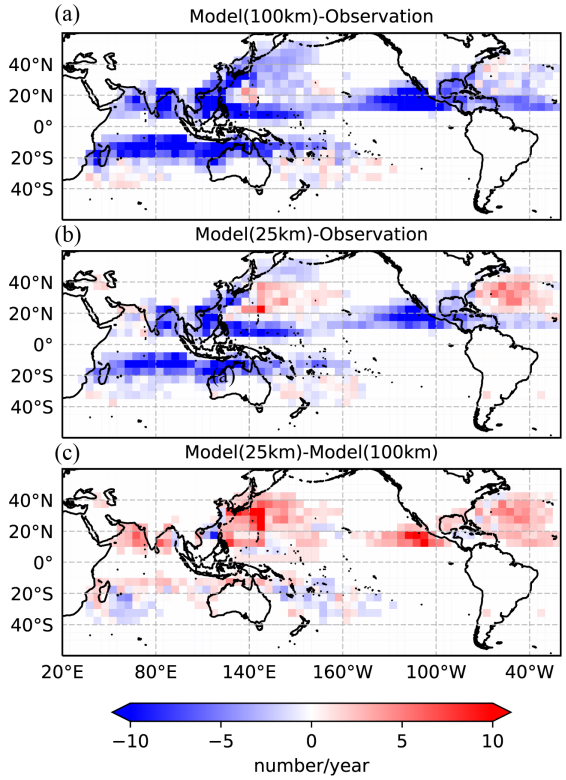

Figure 2. Global track density anomalies of tropical cyclones. The track density is analyzed in (5°×5°) equidistance grid boxes at 6-h intervals and the unit of the color map is the number of cyclones per year from 1991 to 2014. (a) Track density anomaly between FGOALS-f3-L and IBTrACS; (b) track density anomaly between FGOALS-f3-H and IBTrACS; and (c) track density anomaly between FGOALS-f3-H and FGOALS-f3-L.

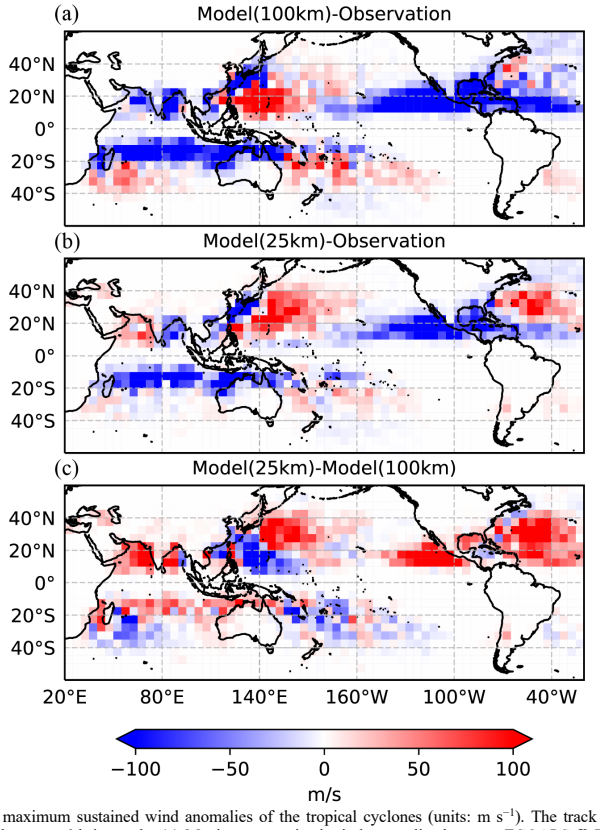

745 **Figure 3.** Global maximum sustained wind anomalies of the tropical cyclones (units: m s^{-1}). The track density is analyzed in (5°×5°) equidistance grid boxes at 6-h intervals. (a) Maximum sustained wind anomalies between FGOALS-f3-L and IBTrACS; (b) maximum sustained wind anomalies between FGOALS-f3-H and IBTrACS; and (c) maximum sustained wind anomalies between FGOALS-f3-H and FGOALS-f3-L.

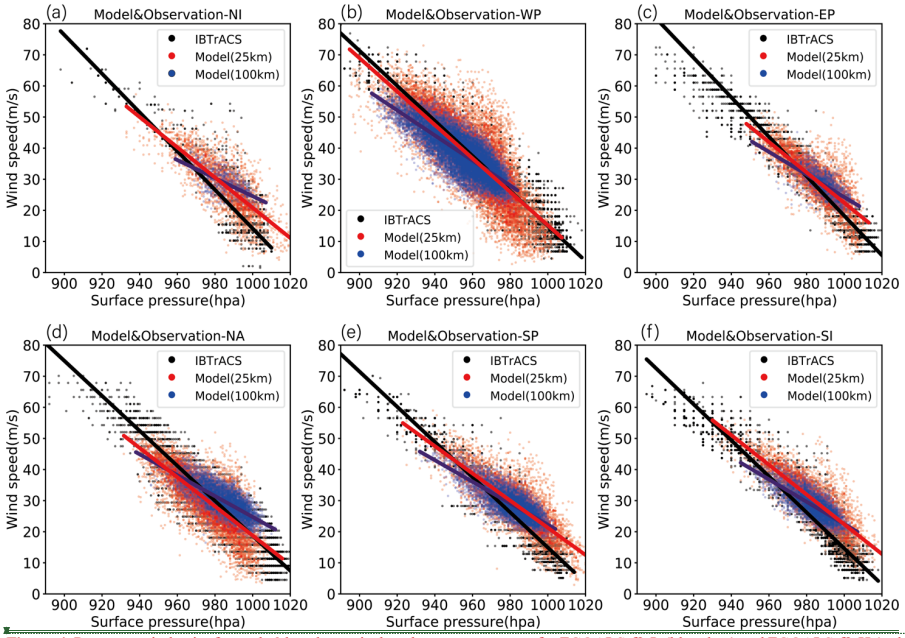

Figure 4. Pressure–wind pairs for each 6-hourly tropical cyclone measurement for FGOALS-f3-L (blue dots) and FGOALS-f3-H (red dots) and IBTrACS (black dots) in (a) northern Indian Ocean, (b) western Pacific, (c) eastern Pacific, (d) northern Atlantic, (e) southern Pacific, and (f) southern Indian ocean. A linear regression (blue/red line for FGOALS-f3-L/H; black line for IBTrACS) is fitted to each distribution of pressure–wind pairs.

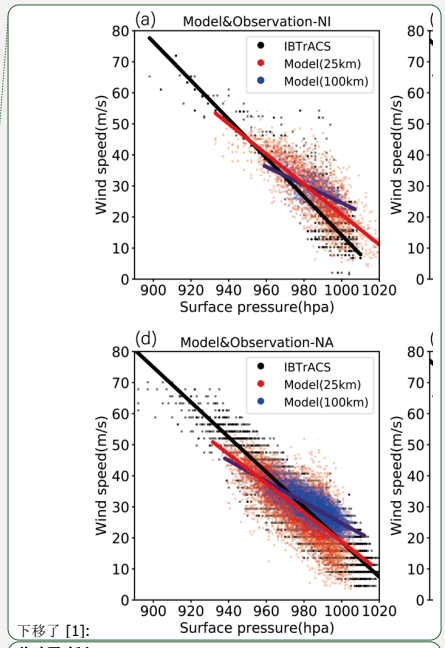

下移了 [1]:

移动了(插入) [1]

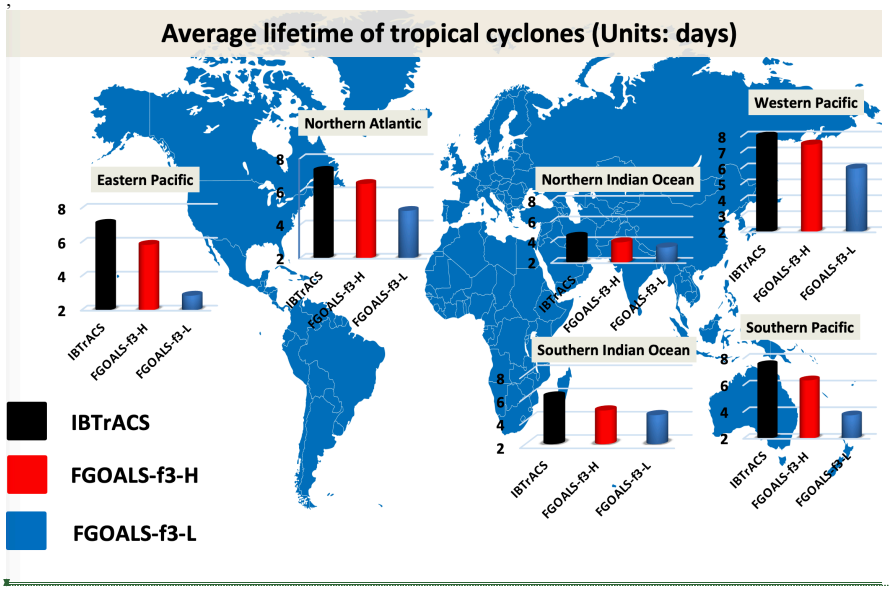

Figure 5. Climatological lifetime of tropical cyclones in the western Pacific, southern Pacific, northern Indian, northern Atlantic, eastern Pacific oceans, and southern Indian oceans (units: days) during the time period 1991–2014.

下移了 [2]:

移动了(插入) [2]

下移了 [9]: **Figure 5.** Climatological lifetime of tropical cyclones in the western Pacific, southern Pacific, northern Indian, northern Atlantic, eastern Pacific oceans, and southern Indian oceans (units: days) during the time period 1991–2014.

移动了(插入) [9]

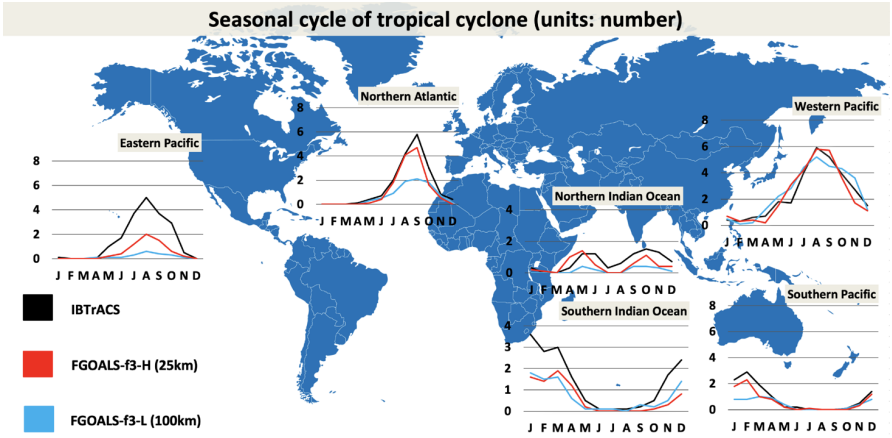

Figure 6. Seasonal cycle of tropical cyclones in the western Pacific, southern Pacific, northern Indian, northern Atlantic, eastern Pacific, and southern Indian oceans (units: number of cyclones) during the time period 1991–2014.

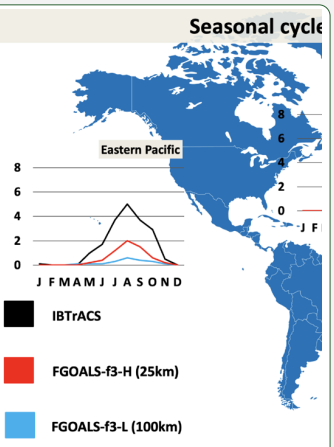

下移了 [3]:

移动了(插入) [3]

下移了 [8]: **Figure 6.** Seasonal cycle of tropical cyclones in the western Pacific, southern Pacific, northern Indian, northern Atlantic, eastern Pacific, and southern Indian oceans (units: number of cyclones) during the time period 1991–2014.

移动了(插入) [8]

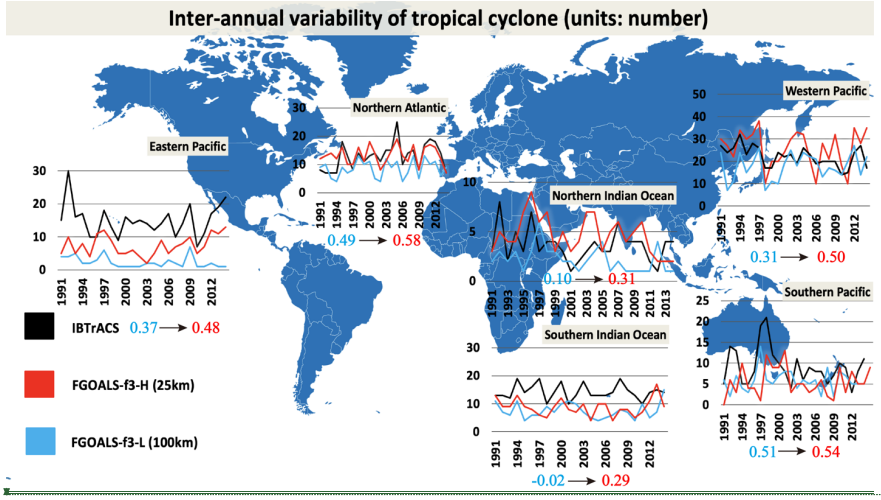

Figure 7. Interannual variability of tropical cyclones in the western Pacific, southern Pacific, northern Indian, northern Atlantic, eastern Pacific, and southern Indian oceans (units: number of cyclones) during the time period 1991–2014. The numbers under the line charts are the correlation coefficients between IBTrACS and FGOALS-f3.

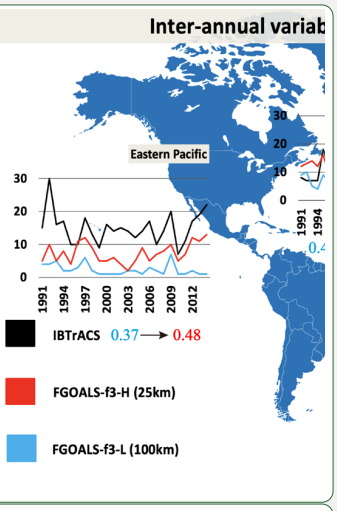

下移了 [4]:

移动了(插入) [4]

下移了 [7]: **Figure 7.** Interannual variability of tropical cyclones in the western Pacific, southern Pacific, northern Indian, northern Atlantic, eastern Pacific, and southern Indian oceans (units: number of cyclones) during the time period 1991–2014. The numbers under the line charts are the correlation coefficients between IBTrACS and FGOALS-f3.

移动了(插入) [7]

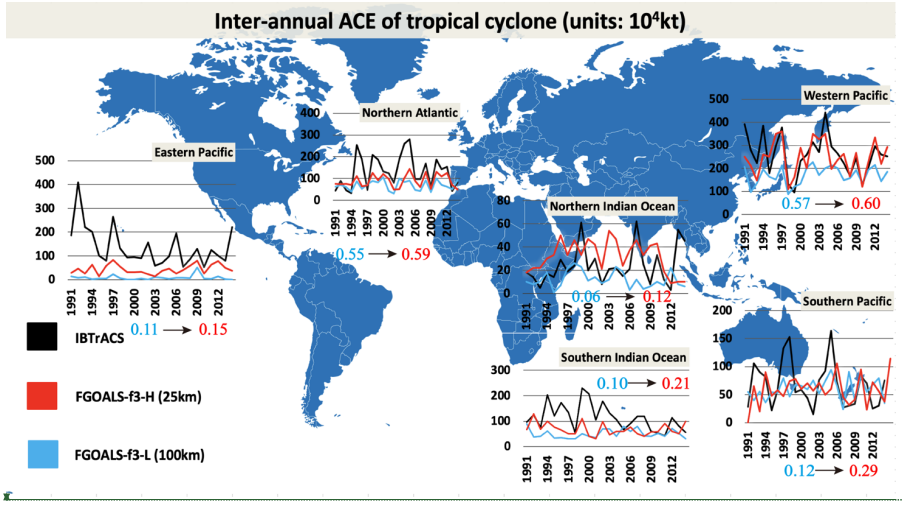

795 **Figure 8.** ACE of tropical cyclones (units: 10^4 kt) in the western Pacific, southern Pacific, northern Indian, northern Atlantic, eastern Pacific, and southern Indian oceans (units: number of cyclones) during the time period 1991–2014.

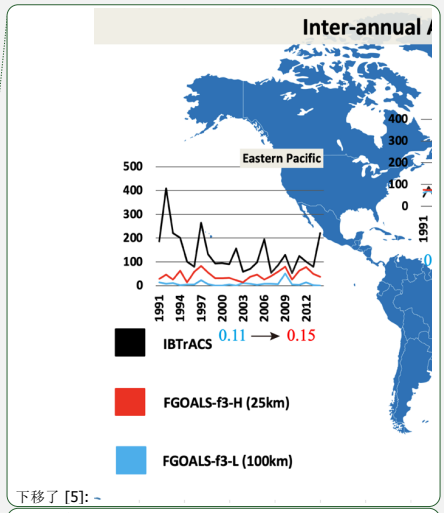

下移了 [5]:

移动了(插入) [5]

下移了 [6]: **Figure 8.** ACE of tropical cyclones (units: 10^4 kt) in the western Pacific, southern Pacific, northern Indian, northern Atlantic, eastern Pacific, and southern Indian oceans (units: number of cyclones) during the time period 1991–2014.

移动了(插入) [6]

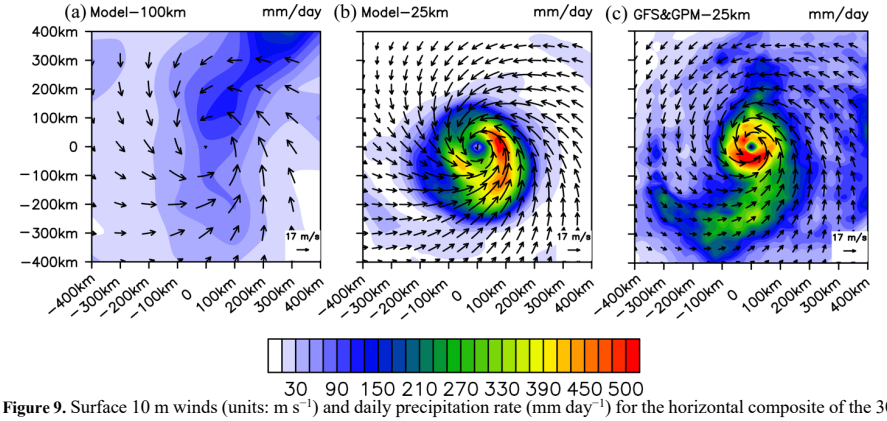

Figure 9. Surface 10 m winds (units: m s^{-1}) and daily precipitation rate (mm day^{-1}) for the horizontal composite of the 30 most intense tropical cyclones in (a) FGOALS-f3-L and (b) FGOALS-f3-H. (c) Results of the surface 10 m wind in GFS and the daily precipitation rate in GPM. Radius is 4°.

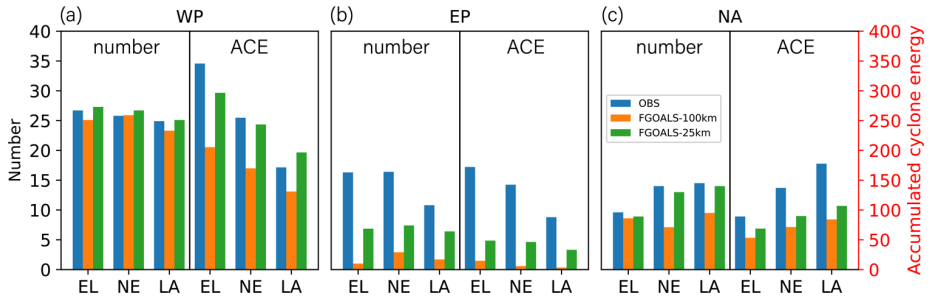

Figure 10. Bar chart showing the average number of tropical cyclones (left-hand panels) and ACE (right-hand panels) from El Niño (EL), neutral (NE) and La Niña (LA) years in the (a) western Pacific (WP), (b) eastern Pacific (EP) and (c) northern Atlantic (NA) oceans.

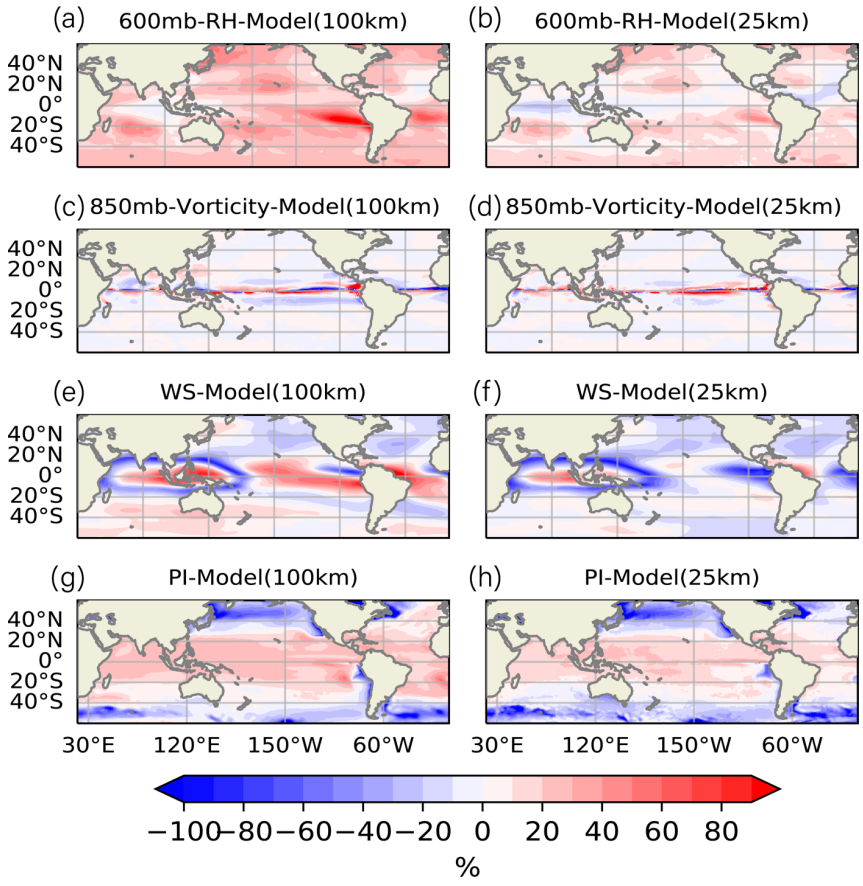

Figure 11. Biases in the large-scale environmental factors related to tropical cyclone activity between FGOALS-f3 and the observations. (a, b) Relative humidity biases at 600 hPa; (c, d) absolute vorticity biases at 850 hPa; (e, f) wind shear biases between 200 and 850 hPa; and (g, h) potential intensity biases.

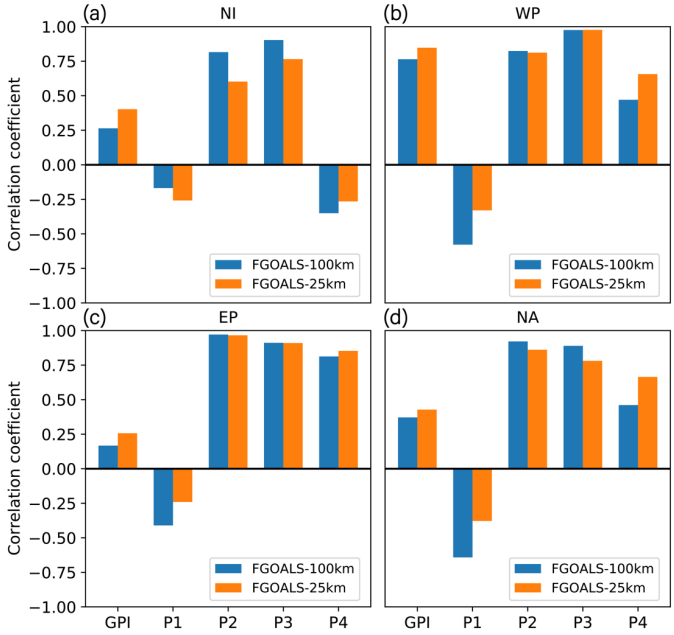

Figure 12. Pattern correlation of annual tropical cyclone GPI between the ERA-Interim dataset and the simulation of FGOALS-f3 at low (blue bars) and high (orange bars) horizontal resolutions in the (a) northern Indian, (b) western Pacific, (c) eastern Pacific and (d) northern Atlantic oceans. P1–P4 represent parts 1–4 of equation 2. P1 represents the equation $|10^5 vort850|^{3/2}$, P2 represents the equation $\frac{RH}{50}$, P3 represents the equation $\frac{V_m}{70}$ and P4 represents the equation $(1 + 0.1V_{\text{shear}})^{-2}$.

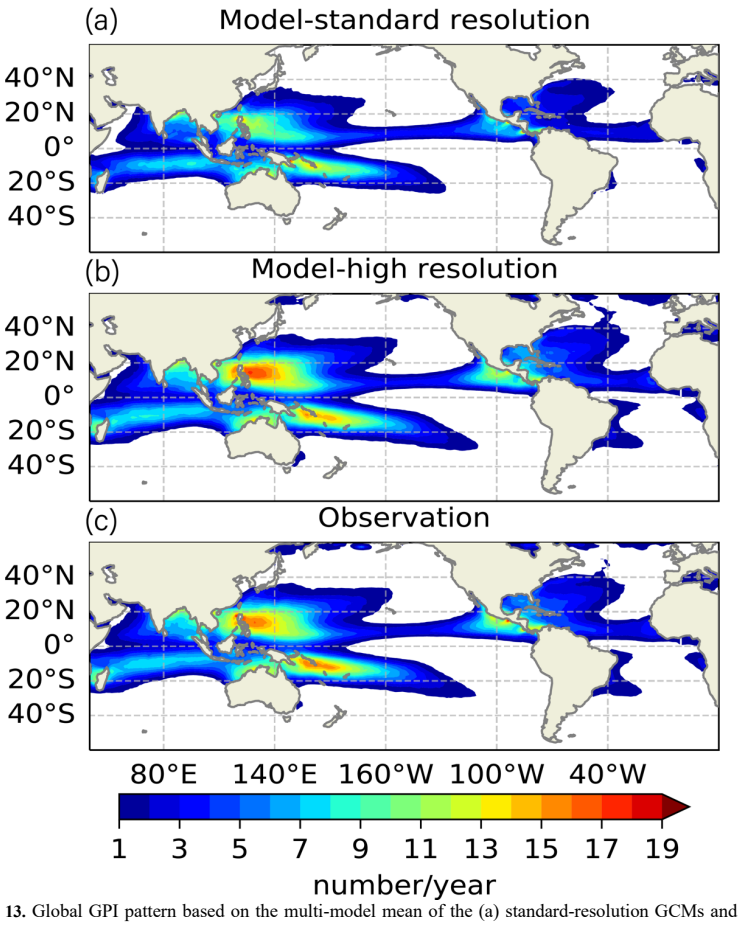

Figure 13. Global GPI pattern based on the multi-model mean of the (a) standard-resolution GCMs and (b) high-resolution GCMs and (c) ERA-Interim dataset.

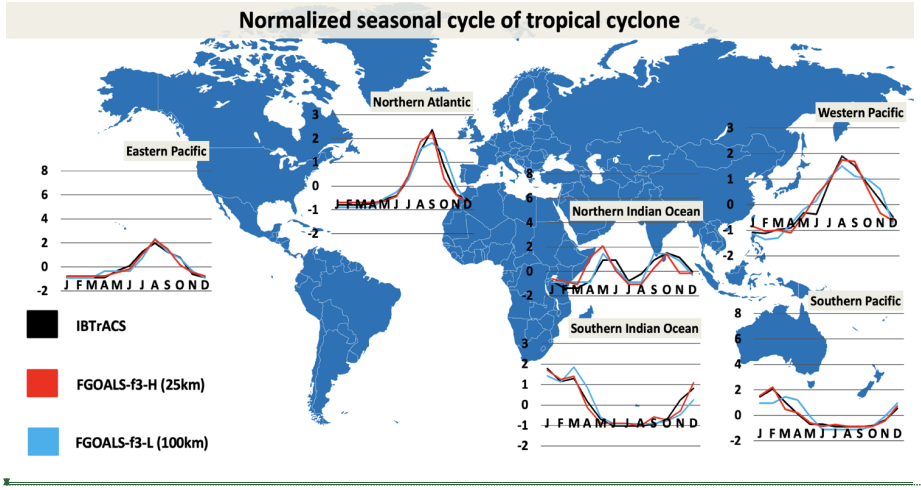

Figure S1. Seasonal cycle of tropical cyclones with zero-mean normalization in the western Pacific, southern Pacific, northern Indian, northern Atlantic, southern Indian, and eastern Pacific oceans (units: number of cyclones) during the time period 1991–2014.

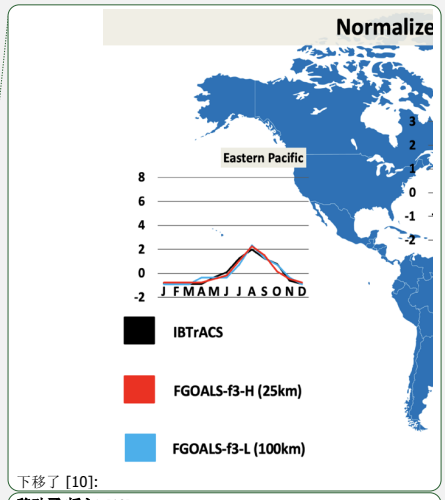

下移了 [10]:

移动了(插入) [10]

删除了: southern Indian